Definition of the Stiesdal Offshore TetraSpar Floating Wind System for OC6 Phase IV

Will Wiley,[1] Roger Bergua,[1] Amy Robertson,[1] Jason Jonkman,[1] Lu Wang,[1] Michael Borg,[2] and Matthew Fowler[3]

1 National Renewable Energy Laboratory
2 Stiesdal Offshore
3 University of Maine

NREL is a national laboratory of the U.S. Department of Energy
Office of Energy Efficiency & Renewable Energy
Operated by the Alliance for Sustainable Energy, LLC

This report is available at no cost from the National Renewable Energy Laboratory (NREL) at www.nrel.gov/publications.

Contract No. DE-AC36-08GO28308

Technical Report
NREL/TP-5700-86442
October 2023

Definition of the Stiesdal Offshore TetraSpar Floating Wind System for OC6 Phase IV

Will Wiley,[1] Roger Bergua,[1] Amy Robertson,[1] Jason Jonkman,[1] Lu Wang,[1] Michael Borg,[2] and Matthew Fowler[3]

1 National Renewable Energy Laboratory
2 Stiesdal Offshore
3 University of Maine

Suggested Citation
Wiley, Will, Roger Bergua, Amy Robertson, Jason Jonkman, Lu Wang, Michael Borg, and Matthew Fowler. 2023. *Definition of the Stiesdal Offshore TetraSpar Floating Wind System for OC6 Phase IV*. Golden, CO: National Renewable Energy Laboratory. NREL/TP-5700-86442. https://www.nrel.gov/docs/fy24osti/86442.pdf.

NREL is a national laboratory of the U.S. Department of Energy
Office of Energy Efficiency & Renewable Energy
Operated by the Alliance for Sustainable Energy, LLC

This report is available at no cost from the National Renewable Energy Laboratory (NREL) at www.nrel.gov/publications.

Contract No. DE-AC36-08GO28308

Technical Report
NREL/TP-5700-86442
October 2023

National Renewable Energy Laboratory
15013 Denver West Parkway
Golden, CO 80401
303-275-3000 • www.nrel.gov

NOTICE

This work was authored in part by the National Renewable Energy Laboratory, operated by Alliance for Sustainable Energy, LLC, for the U.S. Department of Energy (DOE) under Contract No. DE-AC36-08GO28308. Funding provided by the U.S. Department of Energy Office of Energy Efficiency and Renewable Energy Wind Energy Technologies Office. The views expressed herein do not necessarily represent the views of the DOE or the U.S. Government.

Cover Photos by Dennis Schroeder: (clockwise, left to right) NREL 51934, NREL 45897, NREL 42160, NREL 45891, NREL 48097, NREL 46526.

Foreword

The Offshore Code Comparison Collaboration, Continued, with Correlation, and unCertainty project, is an international effort to verify and validate floating offshore wind modeling tools. Phase IV of the project focuses on modeling a novel platform design, the Stiesdal Offshore TetraSpar. All necessary information for reproducing the Phase IV simulations is included in this document, both for project participants and future verification and validation efforts.

Detailed descriptions of the hull, keel, keel lines, tower, turbine, and catenary mooring system are provided. This includes dimensions, mass, inertia, structural properties, and operating conditions. The specification of the device is based on the scaled version used in model tests performed at the University of Maine in 2018–2019. The numerical models are intended to be as similar to the experiment as possible for effective validation comparisons; possible sources of uncertainty in the experiment are identified. Descriptions of the physical tests are provided, including some summary response values. The intended load cases for the numerical effort are prescribed. These include equilibrium, free decay, wind only, wave only, and combined wind and wave conditions. The wind and wave environments are defined both statistically and with measured time series.

Acknowledgments

The authors would like to thank the TetraSpar Demonstrator ApS Consortium consisting of Shell, RWE Renewables, TEPCO RP and Stiesdal Offshore for sharing the scaled TetraSpar for use in this verification and validation effort. We would also like to thank the University of Maine for providing the model test data and thorough experiment description to enable accurate numerical modeling and validation comparisons.

List of Acronyms

CAD	computer-aided design
CC	central column
COG	center of gravity
DB	diagonal brace
DOE	U.S. Department of Energy
EA	modulus of elasticity multiplied by cross-sectional area
FL	fairlead
HT	hull triangular brace
I	mass moment of inertia
KC	Keulegan-Carpenter
KL	keel line
KT	keel triangular brace
MWL	mean water line
OC6	Offshore Code Comparison Collaboration, Continued, with Correlation, and unCertainty
RB	radial brace
RNA	rotor nacelle assembly
YB	yaw bridle

Table of Contents

List of Figures

List of Tables

1 Introduction

The Offshore Code Comparison Collaboration, Continued, with Correlation, and unCertainty (OC6) is an international project focused on verifying and validating modeling tools used in the analysis of floating offshore wind systems. The fourth phase of the project aims to assess the ability of the tools to model a novel floating wind design.

The TetraSpar was selected as the subject platform for the project. This structure was designed by Stiesdal Offshore. The platform is a unique design that features spar-like stability with a very low center of gravity, but does not require rare deep-water ports. This combination is achieved with a system made of two separate steel structures, a hull at the water's surface that supports the wind turbine tower, and a keel that is suspended below the main body. This lower keel has a very high density and drives the total platform's low center of gravity. During assembly in port, using quayside cranes, the keel does not need to be deployed at full depth, allowing the use of many more potential ports. Another unique goal of Stiesdal Offshore was to create a design that consisted of readily manufacturable tubular steel members that need limited-to-no welding during assembly. The TetraSpar, with hull and keel, spar-type stability, and relatively slender components, is unique compared to platforms studied in earlier phases of OC3–OC6 projects, and it offers an opportunity to evaluate the applicability of modeling tools to a novel design, especially hydrodynamic modeling approaches.

A full-scale construction of the TetraSpar was deployed offshore Norway in 200-m deep water in 2021. The platform supports a 3.6-MW Siemens Gamesa Renewable Energy wind turbine and is fully operational. Photos from the construction and commissioning of the platform are shown in Figure 1 and Figure 2; these images are from the TetraSpar Demonstrator Project ApS (Stiesdal Offshore 2023).

Figure 1. Full-scale TetraSpar assembly in Grenaa, Denmark (Stiesdal Offshore 2023)

Figure 2. Full-scale TetraSpar operating offshore Karmøy, Norway (Stiesdal Offshore 2023)

Scaled model tests of the TetraSpar design were performed in 2018–2019 by the University of Maine. The tests were performed with 1:43 Froude scaling. The data collected in the model tests provides a detailed description of the response of the platform in various controlled and relatively well understood conditions. Comparison with this data provides a good opportunity for validation of numerical models. The OC6 Phase IV work will focus on the specific parameters used in these scaled model tests.

Descriptions of the platform and the test campaign in this document are based on the report written by Allen and Fowler of the University of Maine in 2019 (Allen and Fowler 2019).

2 Model Test Description

2.1 Facilities

Model tests were performed in the W^2 wave basin, which is a part of the University of Maine's Advanced Structures and Composites Center. The facility has the capability to create scaled wind and wave environments using a 16-paddle wave maker and rotatable wind machine. Figure 3 shows an elevation view of the facility, which features a moveable floor and a wave damping beach opposite of the wave maker. The basin is 30 m long, 9 m wide, and has a maximum depth of 4.5 m. Tests were performed with the movable floor at its lower limit corresponding to a model-scale depth of 4.5 m and a full-scale depth of 193.5 m. The tank contained fresh water with a density of 1000 kg/m^3; the full-scale sea water has a density of 1025 kg/m^3.

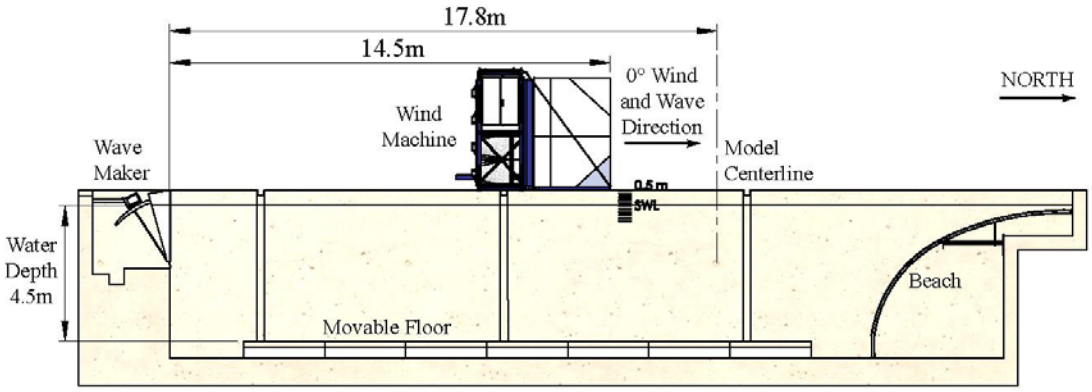

Figure 3. W^2 wave basin elevation (Allen and Fowler 2019)

The wave maker has a maximum wave height of 0.8 m. It has the ability to send waves in the range of -45 degrees to +45 degrees from the tank centerline. Various irregular waves as well as regular waves can be generated. In the TetraSpar test campaign, only head waves were examined, but with a number of different wave heights, periods, and frequency spectra.

The wind machine is capable of generating wind speeds up to 11 m/s and can direct the wind from 0 to 180° relative to the wave direction. In the TetraSpar test campaign, both steady and turbulent winds of different speeds were studied.

Note that all following dimensions and data not describing the model basin are at full scale.

2.2 Measured Data

Data was recorded in the model tests using two systems. Both systems were connected to LabView for data handling.

The first system was made of National Instruments hardware and included wave probes, anemometers, torque gauges, accelerometers, strain gauges, and tension gauges. With the exception of the calibration anemometer, which was sampled at 32 Hz (4.9 Hz full scale), all of this data was sampled at 50 Hz (7.6 Hz full scale).

The second system was a camera-based motion tracking system featuring five cameras above the water and three below the free surface. The cameras followed passive markers and were used to track the position of the hull, keel, and nacelle. This system also recorded information at 50 Hz.

Table 1 lists all of the recorded channels and is categorized by test type and sensor type. A more detailed list of all instruments can be found in Appendix A; this list includes scale factors, sensor model information, and notes.

Table 1. Model Test Data Collection Summary

		Sensor Description	Number of Sensors
Environmental Load Cases	Environment	Time	1
		Wave Elevation Reference Probes	6
		Wind Speed Reference Probe	1
		Wave Maker Paddle Position	9
	Position	Nacelle 6 Degrees of Freedom	5
		Keel 6 Degrees of Freedom	3
		Hull 6 Degrees of Freedom	8
	Turbine	Turbine Torque	1
		Rotor Speed	1
	Tower	Tower Top Acceleration	3
		Tower Base Acceleration	3
		Tower Base Moment	2
	Line Tension	Mooring Fairlead Tension	3
		Keel Tendon Tension	6
		Fairlead Tension (Added Yaw Bridle Connection)	2
	Strain	Hull Strain Gauge	6
Wave Calibration	Environment	Time	1
		Wave Elevation Reference Probes	6
		Wave Elevation Calibration Probes	3
		Wave Maker Paddle Position	9
Wind Calibration	Environment	Time	1
		Wind Speed Reference Probe	1
		Wind Speed X Calibration Probe	1
		Wind Speed Y Calibration Probe	1
		Wind Speed Z Calibration Probe	1

Figure 4 shows the locations of the instruments on the platform. “LC” refers to a tension sensor, either in line with a keel line or a mooring line. “SGRB” refers to a strain gauge.

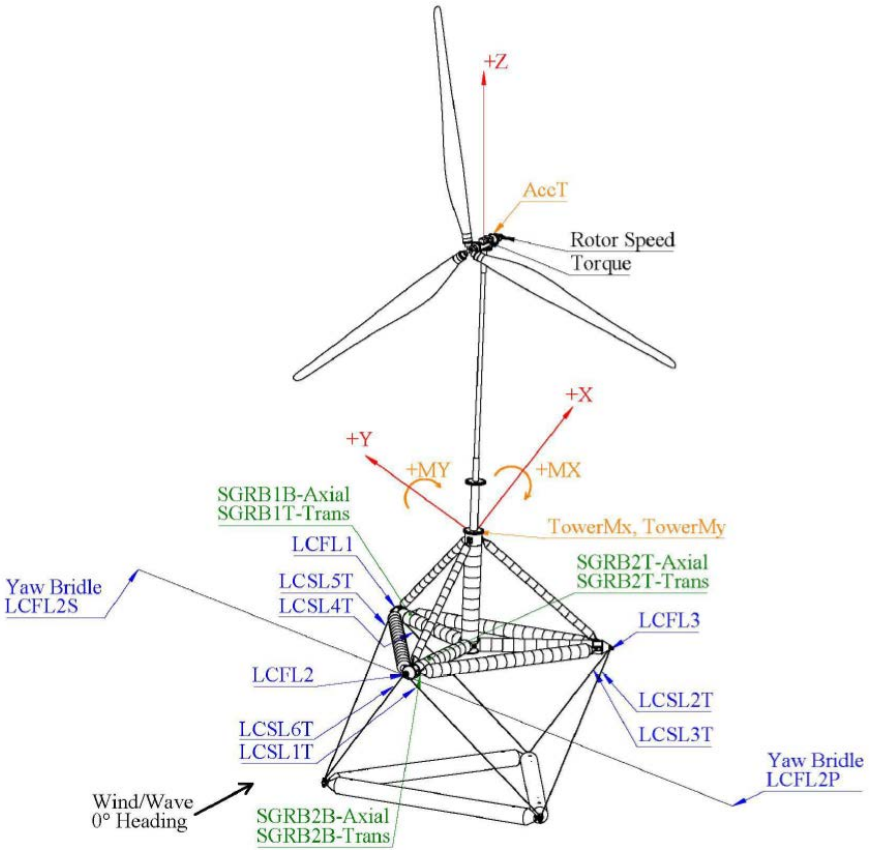

Figure 4. Platform instrument locations (Allen and Fowler 2019)

Environmental loads consisted of wind and waves. Both the wind and wave conditions were calibrated with no turbine or platform present. Figure 5 shows the locations of the wave probes and anemometers used in these tests. Instruments with "ref" in the name were also present for the environmental load cases, while instruments with "cal" in the name were only present in the calibration runs. Calibration Wave Probe 3 is closest in position to the undisplaced platform. Note that x-coordinates in this figure are relative to the tank wave maker; the platform's origin is 781 m downwind of this coordinate system.

In addition to the wave elevations at the probes, the positions of the paddles of the wave maker were also recorded. The calibration wind speed probe recorded the speed separately in the x, y, and z directions, while the reference probe only recorded the magnitude.

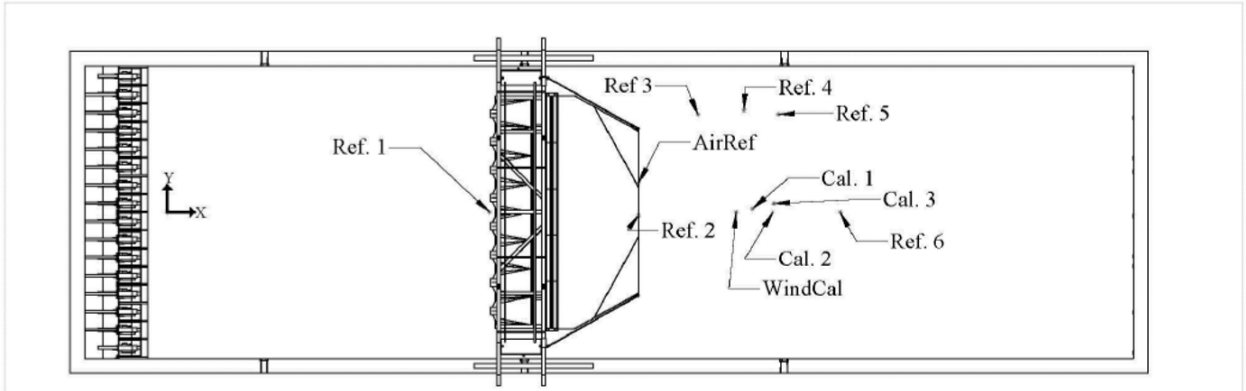

Sensor	X	Y	Z
Ref Anemometer	623.5	38.7	30.1
Cal Anemometer	752.5	0	93.7
WaveProbeRef1	426.1	0	
WaveProbeRef2	623.5	-4.3	
WaveProbeRef3	701.8	129.4	
WaveProbeRef4	763.3	135.0	
WaveProbeRef5	808.4	129.9	
WaveProbeRef6	890.1	0	
WaveCal1	774	4.5	
WaveCal2	802.2	11.6	
WaveCal3	802.2	-1.3	

Full Scale

All measurements in meters

Figure 5. Wind and wave calibration instruments (Allen and Fowler 2019)

2.3 Test Matrix

System identification, environmental calibration, and environmental load cases were run in the test campaign. A limited subset of these tests is used for comparison with numerical simulations.

System identification tests included turbine characterization, static offsets, and free decays. Turbine characterization tests were used to determine the appropriate wind speed and rotor speed for each wind condition. In these tests, the platform was fixed, and wind was created with no waves to isolate the performance of the wind turbine. Particular focus was placed on developing an operating profile that resulted in the desired scaled thrust values. Table 2 lists each of the wind cases tested. Only Wind 1–3 are considered for numerical simulations.

Table 2. Wind Condition Settings (Allen and Fowler 2019)

Wind ID	Description	Pitch Angle Set Point (Blade: A, B, C) [deg]
1	**Rated**	**-6.3, -6.2, -6.2**
2	**Post-Rated**	**18.5, 18.7, 18.8**
3	**50-yr Storm**	**89, 89, 89**
4	2000-yr Storm	89, 89, 89
5	2000-yr Storm Yaw Fault	89, 89, 89

Static offset tests were performed to characterize the catenary mooring system; these were done in the surge and sway degrees of freedom and with no wind or waves. Three unique mooring configurations were examined in each degree of freedom. The body position and the tension at

each fairlead were recorded for each test. Table 3 lists the different static offset tests conducted and the number of offsets for each arrangement.

Table 3. Static Offset Test Matrix

	Number of Offsets	
	Surge	Sway
Base Mooring	3	3
Mooring Without Sensor Umbilical	1	1
Mooring With Yaw Bridle	3	3

Free decay tests were performed to detect the system's natural frequencies and damping values. These tests were done with no wind or waves present and no operation of the turbine. Decay tests were done for all six rigid body degrees of freedom. Three different mooring configurations were studied for each of the decay types; the details of these mooring setups are described in Section Mooring System. Table 4 lists the different conducted free decay tests and the number of decays for each arrangement. The surge equilibrium position of the platform in the decays was significantly different than observed in the wind and wave load cases, thereby likely impacting the mooring stiffness.

Table 4. Free Decay Test Matrix

	Surge	Sway	Heave	Roll	Pitch	Yaw
Base Mooring	16	16	11	10	11	16
Mooring Without Sensor Umbilical	15	15	10	10	10	15
Mooring With Yaw Bridle	16	15	11	10	9	16

Table 5 lists the resulting natural frequencies for each degree of freedom for two of the mooring configurations. The damping ratio is calculated with a PQ analysis.

Table 5. Full-Scale System Natural Frequencies and Damping

	Natural Frequency [Hz]		Damping Ratio
	Base Mooring	Mooring Without Umbilical	Base Mooring
Surge	0.0073	0.0030	22.9%
Sway	0.0044	0.0037	14.8%
Heave	0.025	0.024	4.04%
Roll	0.029	0.029	2.30%
Pitch	0.030	0.029	4.90%
Yaw	0.0070	0.0060	16.2%

Calibration tests were used to understand the incident environmental loads. The platform's interactions with the wind and waves have an impact on measured wind and waves, so the calibration tests were done with no platform present. This validates that the conditions actually created by the wave and wind maker are as expected and gives a high-resolution true time series

of the incident loads. This time series is required both for numerical model comparisons but also for experimental transfer function calculations.

Table 6 lists all of the wind calibration tests, including wind speed and turbulence intensity. Note that the measured wind speed for the yaw fault case is significantly lower than specified. This was done intentionally to most accurately match the scaled thrust of a turbine with a 90° yaw fault; the scaling of the blades resulted in proportionally larger chord lengths, which led to too large of thrust in the fault state for a given wind speed. The highlighted wind conditions are those used in numerical model comparisons.

Table 6. Full-Scale Wind Calibration Test Matrix (Allen and Fowler 2019)

Wind Description	Turbulence	Mean Wind Speed [m/s]	Turbulence Intensity [%]
Rated	**Steady**	**9.89**	**2.40**
Post-Rated	**Steady**	**24.05**	**2.51**
50-yr Storm	Steady	44.62	2.57
2000-yr Storm	Steady	53.08	2.52
50-yr Storm	**Turbulent**	**45.22**	**8.89**
2000-yr Storm	Turbulent	51.78	8.14
50-yr Storm Yaw Fault	Turbulent	33.61	10.99

Turbulent winds were only used for the extreme storm cases, and not the operational cases; however, some turbulence is always present in the wave basin, as shown in the measured values. The turbulence spectra in the turbulent cases were based on the Norwegian Petroleum Directorate, which has uniform spatial coherence. The spectra were created by Stiesdal Offshore combining this model with environmental statistics for the TetraSpar in a 50-yr and 2000-yr storm (Allen and Fowler 2019).

The wave conditions are listed in Table 7. Measured values were recorded with the wave probe WaveCal1, except for the irregular 2000-yr storm wave, which had a sensor failure and used WaveCal3. For all statistical values listed in Table 7, the initial portion of the time series was ignored. Note that only the bolded wave conditions in highlighted cells are used for comparison with numerical simulations.

Table 7. Full-Scale Wave Calibration Test Matrix (Allen and Fowler 2019)

Description	Spectrum	Wave Height [m]	Period [s]	KC Number		λ / D	
				Min.	Max.	Min.	Max.
Rated	**Torsethaugen**	**1.46**	**6.73**	**2.37**	**1.07**	**36.5**	**16.4**
Post-Rated	**Torsethaugen**	**8.00**	**12.48**	**12.99**	**5.84**	**125.6**	**56.5**
50-yr Storm	**Torsethaugen**	**12.81**	**15.79**	**20.80**	**9.36**	**200.4**	**90.2**
2000-yr Storm	Torsethaugen	16.28	18.03	26.43	11.89	258.2	116.2
50-yr Storm Long	Torsethaugen	12.77	15.13	20.73	9.33	184.2	82.9
Rated	Torsethaugen	1.54	6.79	2.50	1.13	37.2	16.7
Post-Rated	**Regular**	**8.31**	**12.41**	**13.49**	**6.07**	**124.2**	**55.9**
50-yr Storm	Regular	12.88	15.61	20.91	9.41	195.9	88.2
2000-yr Storm	Regular	15.79	17.63	25.64	11.54	247.6	111.4
Pink Noise Low	Pink Noise	2.95	-	4.79	2.16	-	-
Pink Noise Mid	Pink Noise	5.88	-	9.55	4.30	-	-
Pink Noise High	Pink Noise	7.82	-	12.70	5.71	-	-

Considering just the wave particle motion and the geometry of the members at the free surface, there is a total range in Keulegan-Carpenter number, from 1.1 to 26.4, within the wave matrix. The top end of this range is large compared to a characteristic semi-submersible floating wind platform, highlighting one unique aspect of this novel design. The range in the wavelength-to-diameter ratio is 16 to 258, which is also large compared to many previously analyzed platforms. These ranges highlight the potentially unique hydrodynamics that need to be considered in modeling efforts. It should also be noted that in model scale, the present Reynolds numbers indicate a theoretically laminar boundary layer on the body. This should be considered in the scaling process for the validation of simulation results; viscous related loads should be associated with the model-scale Reynolds number.

Environmental load cases were run with combinations of incident wind and wave conditions tested in the calibration tests. For the operational cases, only steady wind was used in both the regular and irregular tests. For the storm cases, steady wind was used for the regular tests, and turbulent wind was used for the irregular tests. Table 8 shows the matrix of the different tests; the numbers indicate how many repeat runs were done for each loading combination. The bolded numbers in the highlighted cells indicate the tests used for comparison with numerical simulations.

Table 8. Environmental Load Case Test Repeats Matrix

	Regular			Irregular		
	Wave	Wind	Wave + Wind	Wave	Wind	Wave + Wind
Rated	3	1	3	**2**	-	**3**
Post-Rated	**3**	1	**3**	**2**	-	**3**
50-yr Storm	3	1	3	**2**	4	**3**
2000-yr Storm	3	1	3	2	4	2
50-yr Storm Long	-	-	-	-	-	2
50-yr Storm Yaw Fault	-	-	-	2	-	3
Pink Noise Low	-	-	-	2	-	-
Pink Noise Mid	-	-	-	2	-	-
Pink Noise High	-	-	-	2	-	-

For most of the wave-only cases, the rotor was not spinning at an operational speed. For the regular rated wave-only tests, the rotor was spinning at the same rate as it did when rated wind was present. This wind and operating combination likely is not of particular interest.

For the irregular 2000-yr storm wave and wind condition, three repeat runs were tested; however, one of the repeats had a steady wind instead of a turbulent wind. This is why only two runs are considered for this combination.

2.4 Test Results

Repeated runs offer good information to help quantify uncertainty. In general, there was strong repeatability in the model test data. For numerical model validation, it is important to understand the context of the model tests and potential influences on the data.

2.4.1 Wave Transfer Functions

There was relatively strong agreement between the wave transfer functions of surge, heave, and pitch for the largest three environmental conditions. The response in the rated condition produced a significantly different function. This condition sees the largest wind turbine thrust force. Beyond the impact of the turbine aerodynamic loads, it is expected that there are important nonlinear hydrodynamic forces for this design, and a linear transfer function likely is not fully adequate even in the wave frequency range.

2.4.2 Draft Changes

The draft of the platform was recorded visually at the start of a number of the days of testing. This was done looking at draft marks printed on the central column and documented with photographs. This was only done on 6 different days when the umbilical was connected to the turbine.

The motion tracking of the hull could also be used to determine the draft. The camera-driven data records the position of the hull's center of gravity with respect to the still water free surface.

The initial position for this data before any waves or wind have been initiated can be treated as draft data.

Figure 6 shows the position of the hull center of gravity over the dates of the testing from the two different methods of measuring. Both plots show a trend indicating that the platform is sitting higher in the water at the end of the testing than at the start. The maximum range for the initial position of the hull tracking sensor is close to 4.0 m, while the maximum range for the visual observations is about 1.0 m. The observed readings are considered more reliable, indicating some sensor drift in the hull center of gravity tracking system. With this said, there is still evidence that the draft changes throughout the testing. It appears that this change has some correlated trend and is not purely random. Changes in the positioning of the sensor umbilical could be a potential cause of the change, which is sensitive, given the platform's small waterplane area.

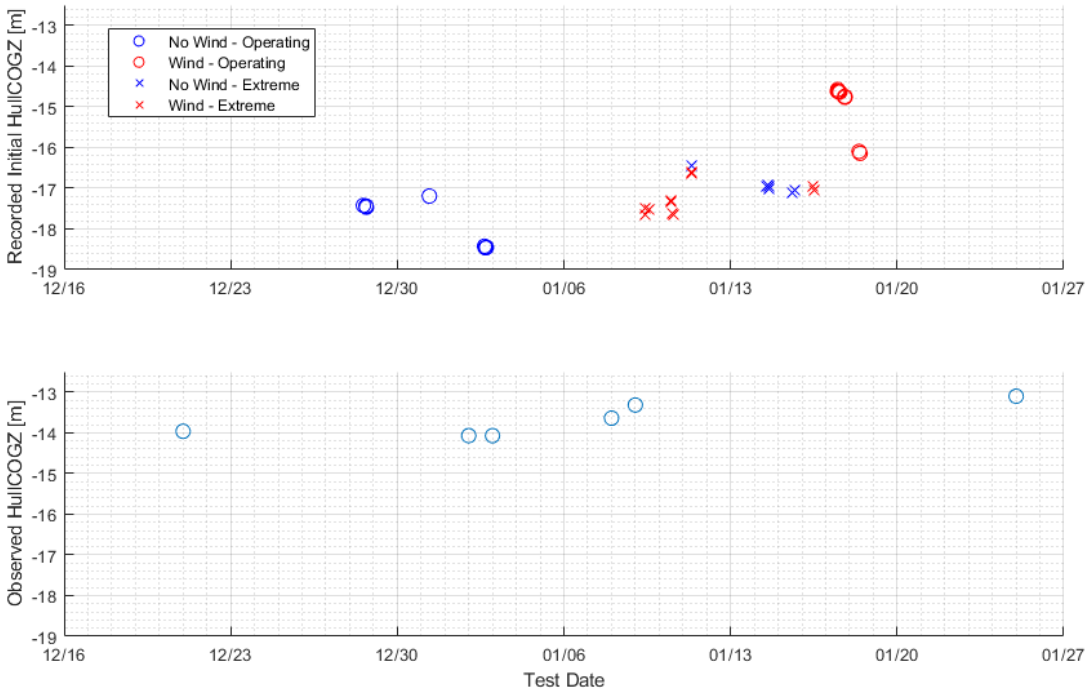

Figure 6. Full-scale draft changes by date

Changes in draft can both affect the dynamic properties of the system and the environmental excitation of the system. In addition to the expected correlation to a change in mass and inertia, there are changes to the water plane area and mooring stiffness. All of these differences could result in varying natural frequencies for each degree of freedom. Given the small waterplane area and cylindrical members, the effects on natural frequencies are not as large as they could be, but they do exist.

Both wave excitation and wind excitation are also influenced by the change in draft. When the horizontal members of the hull and the keel are at different distances below the free surface, they see different wave particle velocities. A platform sitting higher in the water would receive more wave excitation. When the wind turbine rotor is at a different height above the free surface, it is at a different point in the air's jet stream. While no vertical velocity profile in the wind was

intended, some variation could exist, and different vertical positioning of the turbine would impact the aerodynamic excitation and damping of the platform.

The description of the platform in Section Platform is with respect to a tower connection freeboard of 11.3 m. This corresponds to the hull's center of gravity sitting 13.5 m below the free surface, which is the mean observed value during the environmental test cases. The hull center of gravity tracking data shows a mean value of 17.0 m below the free surface. This data was adjusted by 3.5 m to line up with the observed draft readings. In numerical model validation, it may be important to consider differences in this position.

2.4.3 Keel Line Tensions

A particularly interesting aspect of the TetraSpar design is the keel lines interconnecting the hull and keel. The recorded keel line tensions offer a good way to analyze the internal loading between the hull and keel. This is helpful in achieving the goal of the project to assess the applicability of modeling tools to novel designs, including those with substructure flexibility and internal member-level loading.

Analysis of the recorded keel line tension data identifies good consistency between repeated runs. Interestingly, the response is asymmetric between the port and starboard keel lines; this is particularly significant for the two lines furthest downwind and when wind is present. The idling turbine in high wind induces a roll moment. The mean roll offset loads one side of the platform and unloads the other side. This points to the importance of capturing asymmetric loading in numerical models.

3 Modeling Information

The 1/43 scale model of the TetraSpar was built by Stiesdal Offshore for the model tests. Figure 7 shows the model in the wave basin at University of Maine.

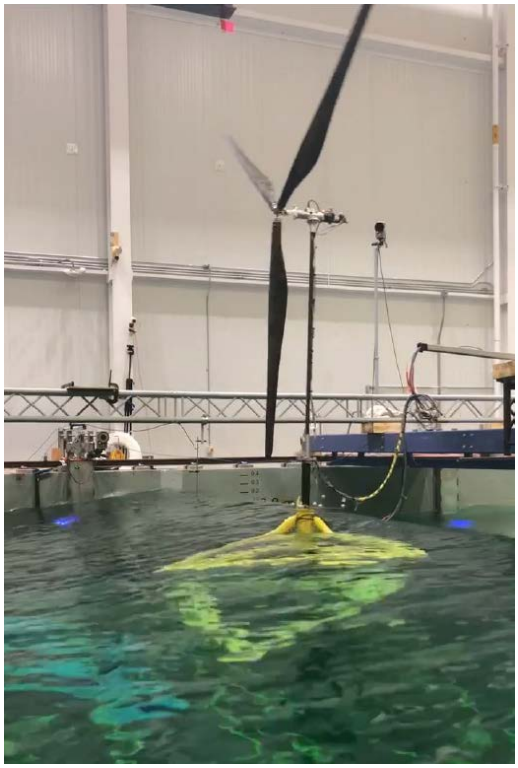

Figure 7. TetraSpar model test in the University of Maine's W² basin during wave test (Allen and Fowler 2019)

3.1 Wind Turbine

A custom-scaled wind turbine was used in the tests. The starting point for the turbine was University of Maine's stock model-scale turbine based on the National Renewable Energy Laboratory's 5-MW design. The turbine was adapted to have the scaled mass, inertia, and thrust properties of the prototype wind turbine. The blades, nacelle, and connections were all made smaller for the desired mass properties. University of Maine notes that, while some other characteristics of the turbine were not matched, particularly for individual components, it is not likely that this will have a significant impact on the global response.

Table 9 contains measured and assumed properties of the wind turbine at full-scale equivalent. The hub height is with respect to the mean waterline (11.3 m below the tower-hull interface). The topside center of gravity is with respect to the tower-rotor nacelle assembly (RNA) connection. The blade center of gravity values are with respect to the blade root. Inertia values are given with respect to the center of gravity of the full RNA.

Table 9. Full-Scale Wind Turbine Properties (Allen and Fowler 2019)

		Test Method	Notes
Hub Height	88.27 m	Measured	With respect to mean water line
Hub Radius	3.40 m		
Rotor Radius	64.50 m		
Rotor Centroid Overhang	-9.68 m	CAD Model	With respect to tower axis
Shaft Tilt	0.0°		
Blade Cone Angle	0.0°		
Complete Topside Mass	2.62e5 kg	Scale	
Complete Topside COG X	-2.65 m	Wedge Test	With respect to tower nacelle interface
Complete Topside COG Y	0.00 m		
Complete Topside COG Z	1.25 m		
RNA I_{XX}	4.42e7 kg-m^2	Swing Test	With respect to RNA COG
RNA I_{YY}	2.70e7 kg-m^2		
RNA I_{ZZ}	5.47e7 kg-m^2		
Nacelle Mass	1.49e5 kg	Scale	
Hub Mass Without Blades	5.57e4 kg		
Blade A Mass	1.95e4 kg		
Blade B Mass	1.86e4 kg		
Blade C Mass	1.87e4 kg		
Blade A Radial COG	22.62 m	Wedge Test	With respect to blade root
Blade B Radial COG	22.53 m		
Blade C Radial COG	23.31 m		
Hub Inertia	3.66e5 kg-m^2	CAD Model	With respect to RNA COG
Hub and Blades Inertia	4.83e7 kg-m^2		

Figure 8 shows the arrangement of the wind turbine assembly, including some of the dimensions from Table 9.

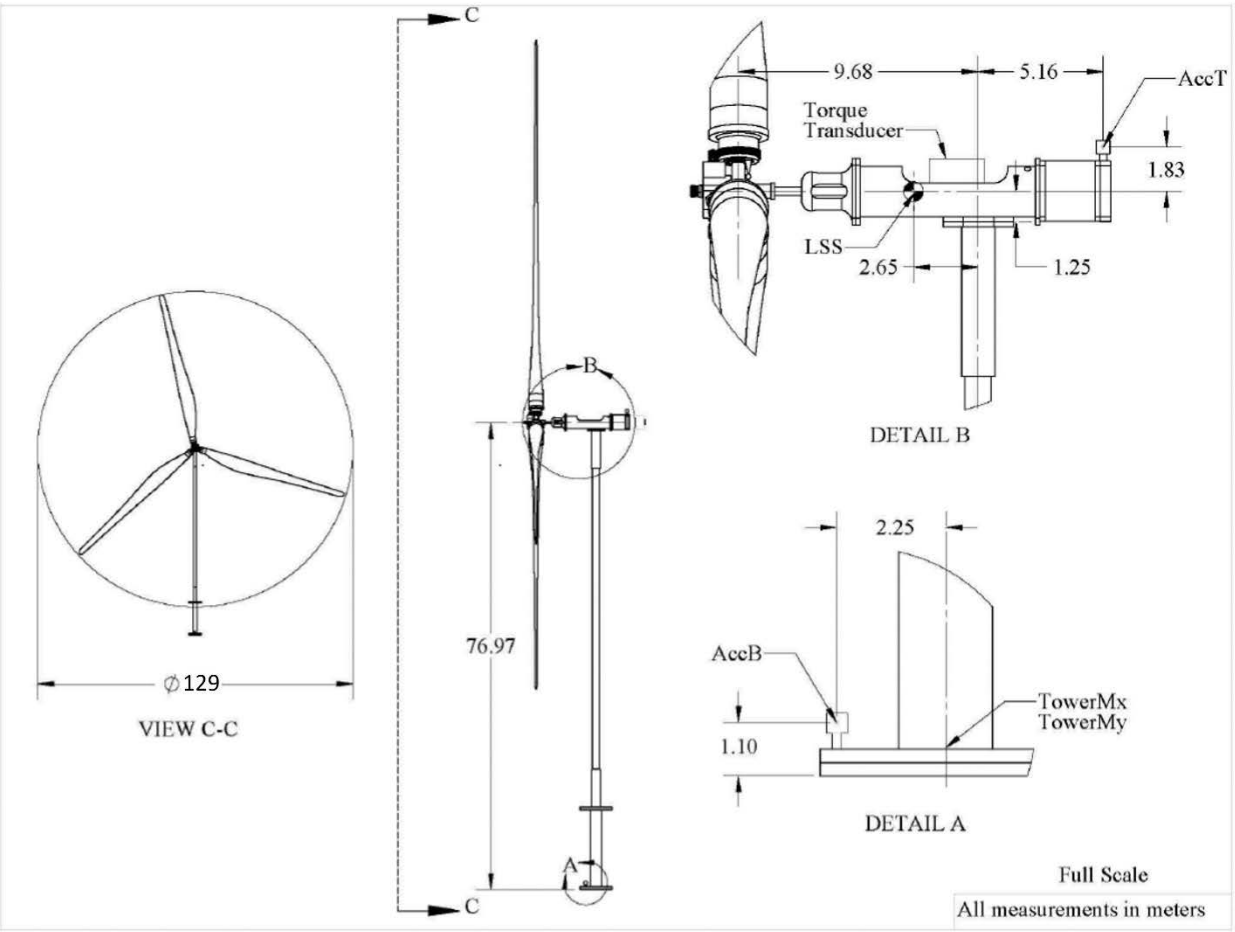

Figure 8. Full-scale wind turbine arrangement (Allen and Fowler 2019)

3.1.1 Rotor

The blades were modified to achieve the desired scaled thrust force for the Siemens 3.6-MW turbine. The blades have a cylindrical section at the root that blends out to an airfoil section named AG04MOD, which is a modified version of the Drela AG04 (Allen and Fowler 2019).

Appendix B contains information about the blades and the airfoils. Table B- 1 contains the aerodynamic coefficients for the AG04MOD foil, and Table B- 2 contains the aerodynamic coefficients for a cylindrical foil. The coefficients were found with the XFOIL code and have not been checked with experiment. Figure B- 1 shows the shape of the AG04MOD foil, which is described by the coordinates listed in Table B- 3. Finally, Table B- 4 describes the progression of the shape and size of the blade cross sections. Note that an angle of twist of 0° indicates a chord line in the rotor plane, and a positive angle of twist indicates an upwind leading edge. It is recommended that aerodynamic coefficients are linearly interpolated between airfoil types in the blended region.

Detailed knowledge of the structure of the blades is not known. For this reason, the blades are to be simply treated as rigid for modeling purposes.

3.1.2 Operation

The operations of the wind turbine and the associated wind conditions were tuned to achieve desired scaled thrust values. This process was done with a set of wind-only thrust characterization tests. Five different cases were considered. Two of these cases are associated with an operating turbine, in a rated and post-rated condition. Three of the cases are associated with extreme storm conditions. The turbine was tested in a normal idling state for a 50-yr storm condition and a 2000-yr storm condition, as well as an idling condition with a 90° yaw fault for the 50-yr storm state.

Figure 9 shows the wind speed, rotor speed, and resulting tower base bending moment for each of the five wind conditions. Note that Conditions 3 and 5 have different wind speeds, even though they represent the same return period storm (50-yr storm and 50-yr storm with yaw fault). These speeds were again uniquely chosen based on tuning to match desired scaled thrust forces that correspond to the case, and not necessarily a scaled wind speed. The rotor is driven at a chosen rotation speed for Operational Conditions 1 and 2. Conditions 3 and 4 see some passive idling low-speed rotation.

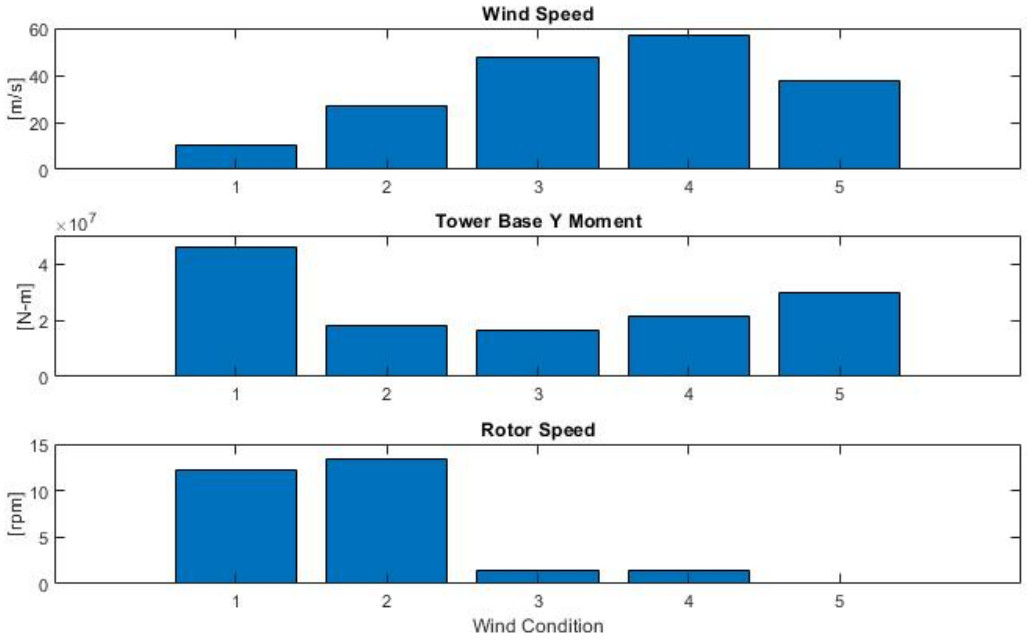

Figure 9. Wind condition characterization tests (full scale)

In the extreme storm conditions with pitched blades and an idling rotor, a significant contribution to the total thrust comes from the tower drag. University of Maine did not have a way to separately measure this tower component of the thrust. They subtracted an analytical tower drag from the thrust, based on the tower base moment, to check for the target turbine thrust in these conditions.

In addition to an adjustable rotor speed, the model turbine has blade pitch actuation. Pitch angle set points were selected for each unique blade construction for each wind condition. All of the storm cases featured fully pitched blades for the idling condition. The selected angles are shown in Table 2.

3.2 Tower

The tower was custom-designed and built to match the desired first fore-aft and side-to-side bending mode frequencies, as well as total mass and center of gravity. The tower consists of sections of aluminum and carbon fiber. Dimensions of each section are shown in Figure 10. Above the second flange and below the third flange (nacelle mount) are sections with a carbon fiber tube inside of an aluminum tube. For modeling purposes, it is assumed that this is a tight connection, and the combined stiffness can simply be thought of as the summation of each component's stiffness in parallel.

The carbon fiber tube was purchased from Grafil Inc. and was made using a roll wrap technique with layers of prepreg carbon fiber with varying fiber orientation.

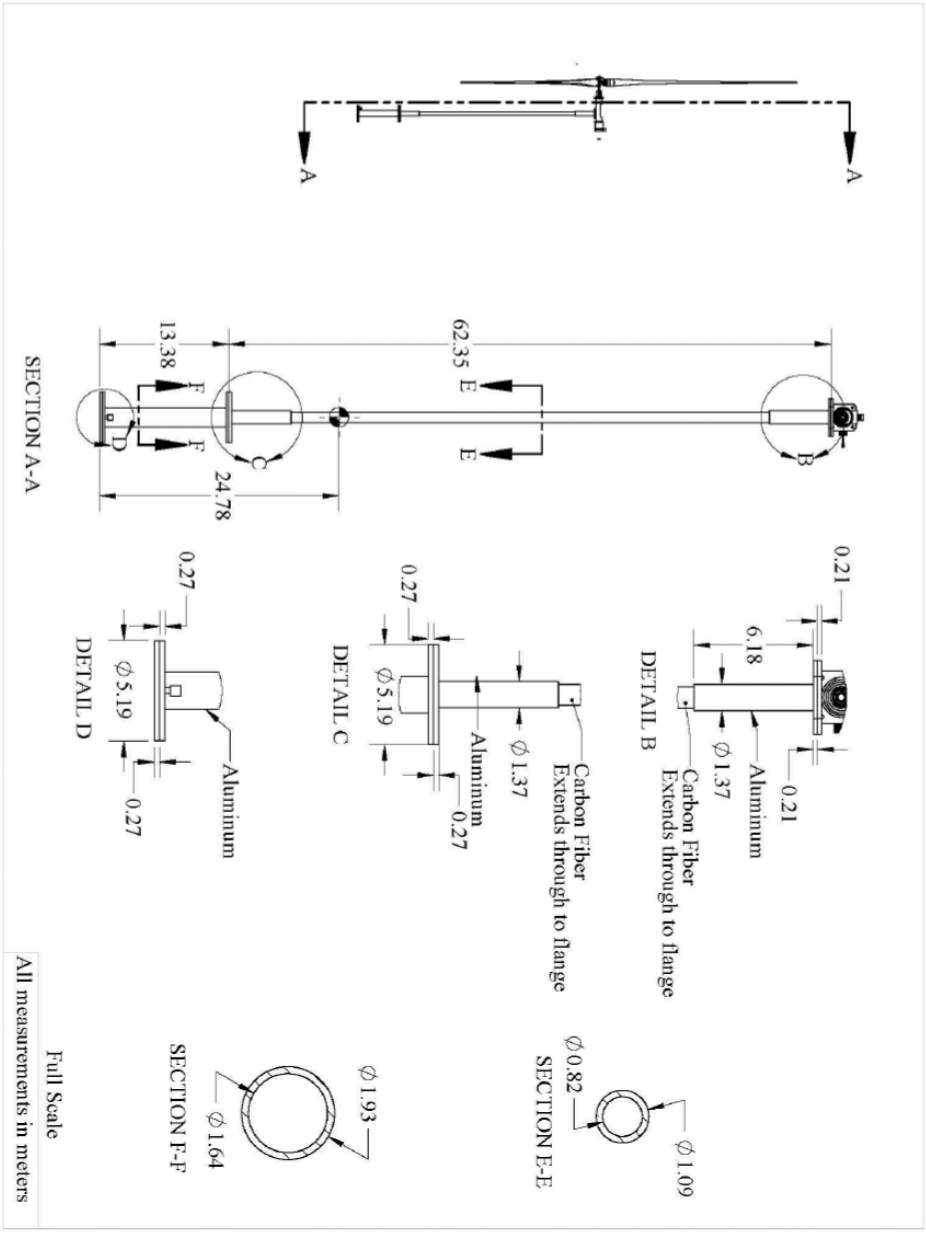

Figure 10. Full-scale tower construction (Allen and Fowler 2019)

Hammer tests were performed to check the bending mode frequencies. The full RNA was present in these tests. The tower was rigidly mounted at the base for these tests, and the bending moments in the fore-aft and side-to-side directions were recorded. In the environmental load cases with a floating platform, it is expected that both the mode shapes and the modal frequencies differ from the hammer tests, given the floating body free-free boundary condition. The results with the rigidly connected base are still useful for model calibration. The frequency spectra of the tower base moments are shown in Figure 11 and Figure 12, and the damping ratios are shown in Figure 13 and Figure 14.

Analysis of the tower base moment response in the irregular environmental load cases suggests that the tower's first bending mode frequency is close to 0.39 Hz with a floating body base boundary condition.

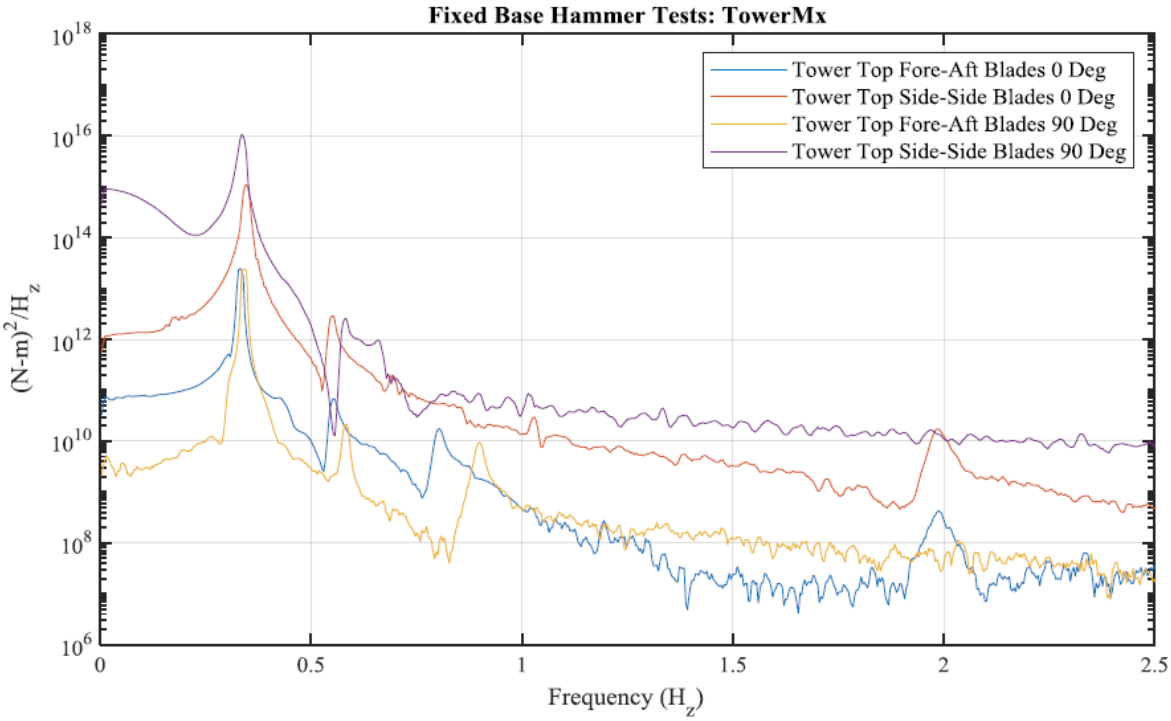

Figure 11. Tower base side-side moment hammer test response (Allen and Fowler 2019)

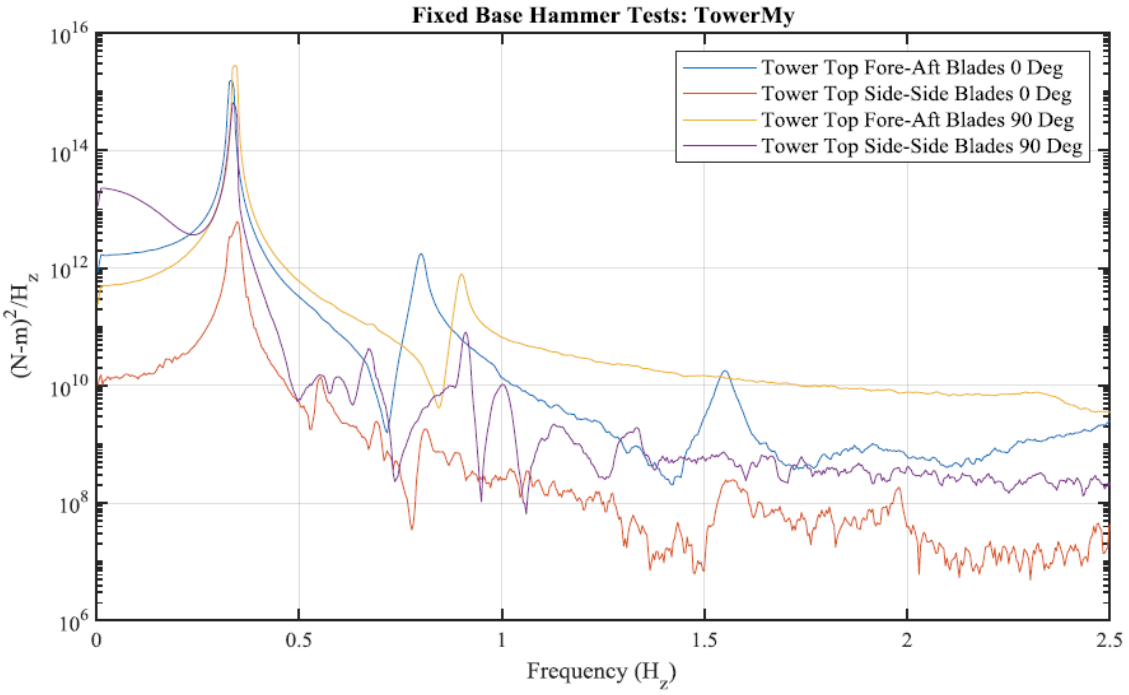

Figure 12. Tower base fore-aft moment hammer test response (Allen and Fowler 2019)

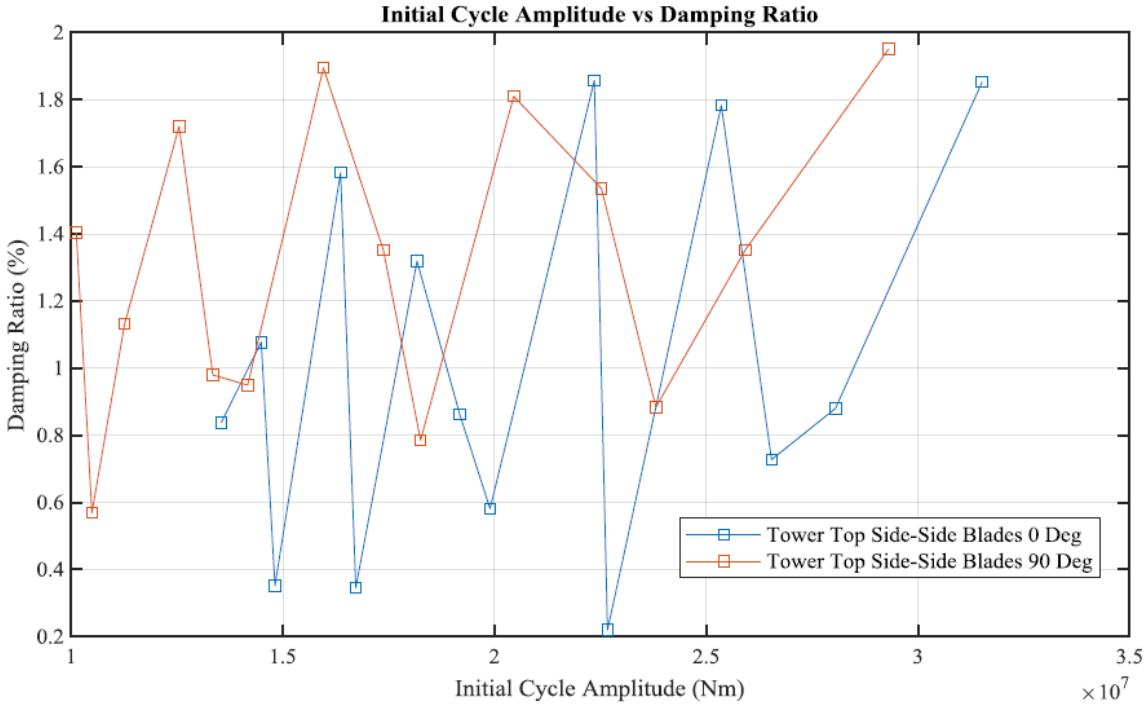

Figure 13. Tower base side-side moment free decay damping response (Allen and Fowler 2019)

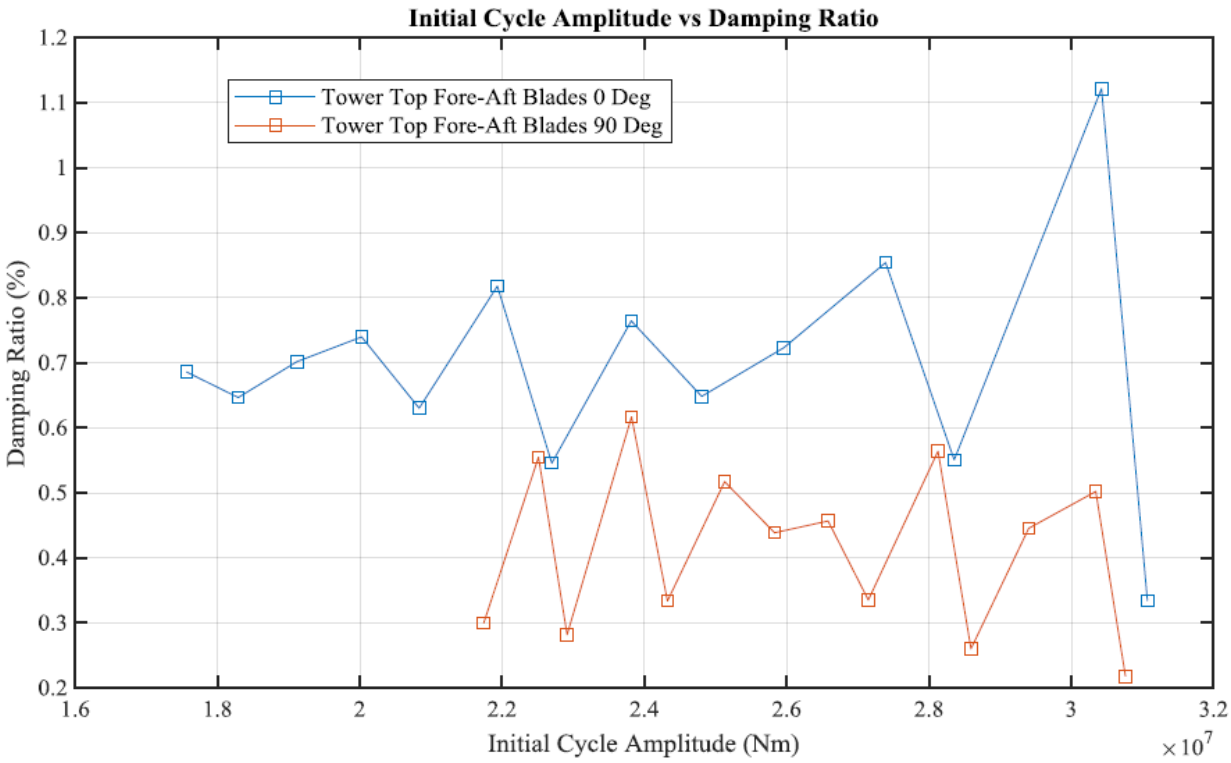

Figure 14. Tower base fore-aft moment free decay damping response (Allen and Fowler 2019)

The measured properties for the complete tower are shown in Table 10. The center of gravity is given with respect to the tower base, and the inertia values are given with respect to the tower center of gravity. It is also assumed that the tower is axisymmetric, and the resulting center of gravity is at the origin in this plane.

Table 10. Full-Scale Measured Tower Properties

	Measured Value	Test Method
Mass	1.51e5 kg	Scale
Z COG	24.51 m	Wedge Test
I_{XX}	8.72e7 kg-m^2	Swing Test
I_{YY}	8.52e7 kg-m^2	Swing Test
I_{ZZ}	2.17e5 kg-m^2	Swing Test
First Fore-Aft Bending Mode Frequency	0.34 Hz	Hammer Test (rigid base)
First Side-Side Bending Mode Frequency	0.35 Hz	Hammer Test (rigid base)

Table 11 gives full-scale material properties for the carbon fiber and aluminum used in the tower model. It was found with the given Young's moduli that the tower model was too stiff. There was some uncertainty in the stiffness for the carbon fiber based on the fiber orientation. This stiffness value was tuned to obtain a tower model that matched the first fore-aft and side-side bending mode frequencies for the fixed boundary condition. This recommended tuned value is also given in the table. The tower frequencies should be independently checked in numerical models, and the tower mode shapes and frequencies in environmental load cases should correspond to the floating body boundary condition.

Table 11. Full-Scale Tower Material Properties

		Scaled	Scaled and Tuned
Carbon Fiber	Density	1640 kg/m^3	
	Stiffness	5730 GPa	2116 GPa
Aluminum	Density	2768 kg/m^3	
	Stiffness	2997 GPa	

Table 12 lists the sectional properties for each segment of the tower. These properties are based on the material properties given in Table 11 and the dimensions from Figure 10. The internal geometry of the flanges is not known, and in these proposed sectional properties, this value is adjusted to match the measured total mass and tower vertical center of gravity. Note that, depending on discretization of the tower, these properties may need to be tuned to match the total tower mass, inertia, center of gravity, and structural frequency. With these properties, the RNA mass, inertia, and a cantilever beam boundary condition, the tower has a first bending mode with a frequency of 0.34 Hz matching the experimental hammer tests. Again, it is most important that the tower mode shape and frequency is correct with a floating boundary condition; this should be checked in each numerical model.

Table 12. Full-Scale Tower Sectional Properties

Section	Description	Lower Limit [m]	Upper Limit [m]	External Diameter [m]	Internal Diameter [m]	Density [kg/m^3]	Stiffness [GPa]
1	Hull Interface Flange	0.0	0.54	5.19	2.20	2768	2997
2	Aluminum Only	0.54	13.11	1.93	1.64	2768	2997
3	Middle Flange	13.11	13.65	5.19	0.00	2768	2997
4	Aluminum + Carbon Lower	13.65	19.83	1.37	0.82	2285	2722
5	Carbon Only	19.83	69.34	1.09	0.82	1640	2116
6	Aluminum + Carbon Upper	69.34	75.52	1.37	0.82	2285	2722
7	RNA Interface Flange	75.52	75.94	3.75	2.82	2768	2997

3.3 Platform

The TetraSpar platform consists of two sections: a roughly tetrahedral hull that pierces the free surface and a triangular keel suspended below the hull by keel lines. Figure 15 shows a perspective view of the platform with labeled members. Each of the members are cylindrical tubes capped with cone-shaped nodes. In the physical construction of the model, the joints at the tip of each node are pins; for numerical simulations, the joints will be treated as rigid connections (because the distributed structural mass and stiffness of the members is not known). The hull consists of a vertical central column (shown as “CC” in the figure) directly beneath the wind turbine tower. At the base of the central column, there are three radial braces (shown as “RB” in the figure) in the horizontal plane spaced 120° apart. Rigidity is given to this base with hull tri braces (shown as “HT” in the figure) and diagonal braces (shown as “DB” in the figure).

The keel is simply made of three tri braces in the horizontal plane. The diameters of each of these members are given in Figure 15. The keel is suspended from the hull by six flexible tendons, denoted as keel lines ("KL" in the figure). The center of the keel is directly beneath the central column of the hull. For OC6 Phase IV participants that can, the keel lines will be modeled flexibly so as to be able to calculate internal keel-line tension for comparison to the measurements.

Member	Diameter	Length
CC	4.3 m	32.15 m
DB	1.935 m	39.95 m
RB	3.44 m	34.93 m
HT	4.3 m	54.76 m
KT	4.3 m	64.30 m

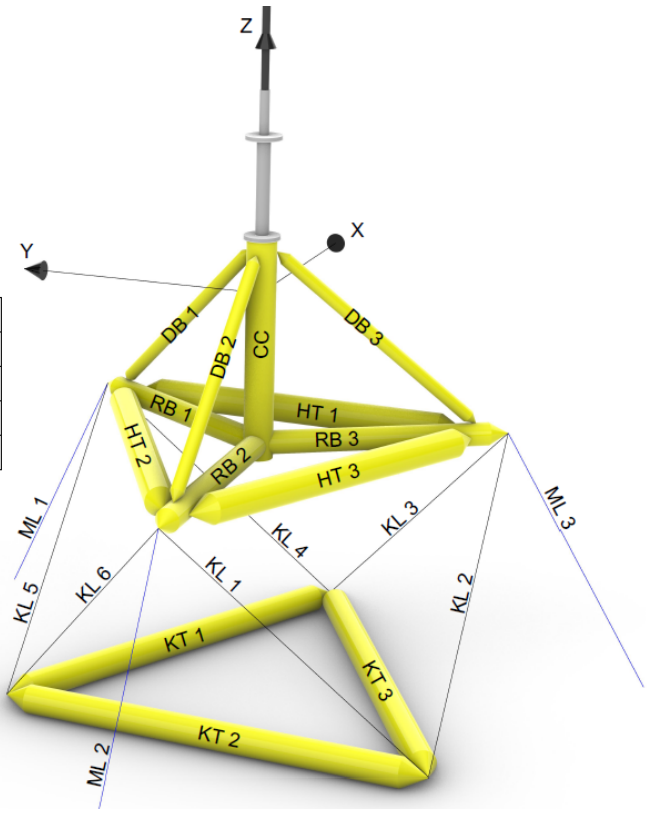

Figure 15. TetraSpar perspective view with full-scale dimensions

The coordinate system in Figure 15 is at the intersection of the still free surface and the center of the central column, 11.3 m directly beneath the tower connection. This coordinate system is used for all platform coordinates and the origin for platform motions. Wind and waves propagate in the positive x-direction in environmental load cases. Repeated members are numbered starting at the positive x-axis and moving in a counter-clockwise direction when viewed from above. The keel line numbering begins in the opposite quadrant.

Figure 16 shows a side view of the TetraSpar with dimensions. The waterline is set to the mean value from the environmental load cases. This results in a freeboard of 11.3 m to the tower connection. The dashed black lines run through the centerlines of the corresponding members. These indicate that the centerlines of the diagonal braces intersect the center of the central column at the tower connection and the radial braces at the start of the node. The centerlines of the hull tri braces also intersect the radial braces at the same point, where the node begins.

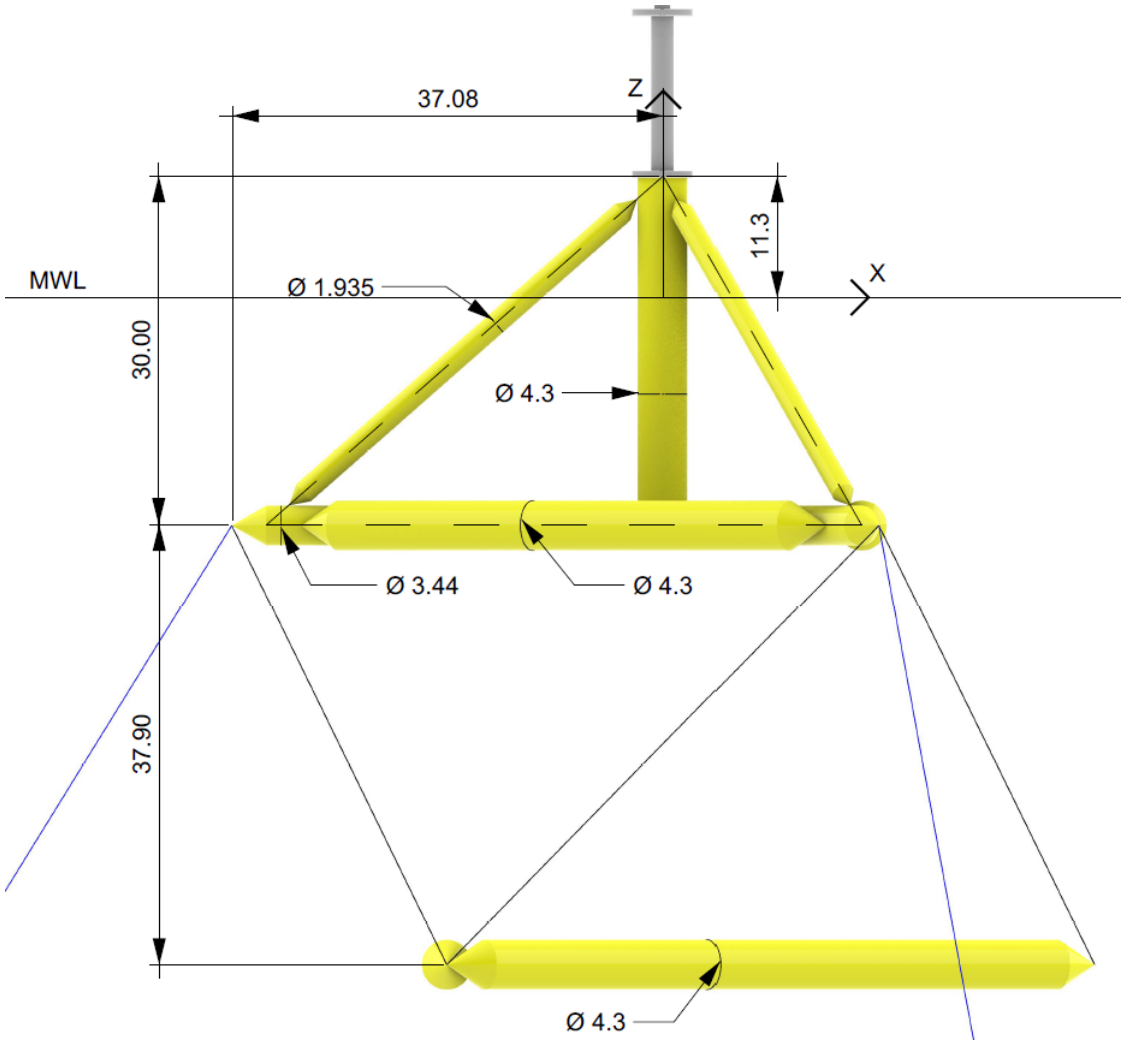

Figure 16. TetraSpar side view with full-scale dimensions

Appendix C gives the coordinates of the joints at the ends of each member, as shown in the side view. The z-coordinates are consistent with the 11.3-m tower connection freeboard.

Figure 17 shows a top view of the TetraSpar. There is a 60° rotation between the base triangles of the hull and the keel. This configuration with the six keel lines creates a stiff stable system.

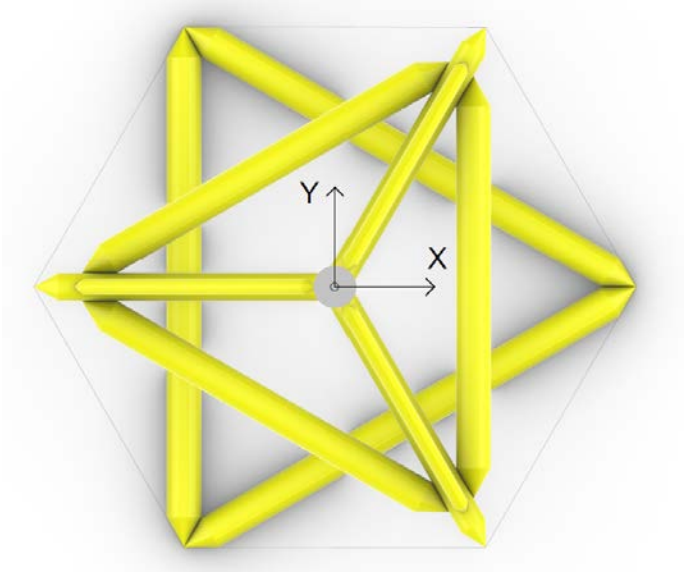

Figure 17. TetraSpar top view

Figure 18 shows a front view of the TetraSpar, looking in the downwind direction. There is a small difference in the outer extents of the hull and the keel. At this draft, the TetraSpar has a relatively low freeboard at the tower connection. There is potential for some surface-piercing members to become fully submerged in extreme wave load cases.

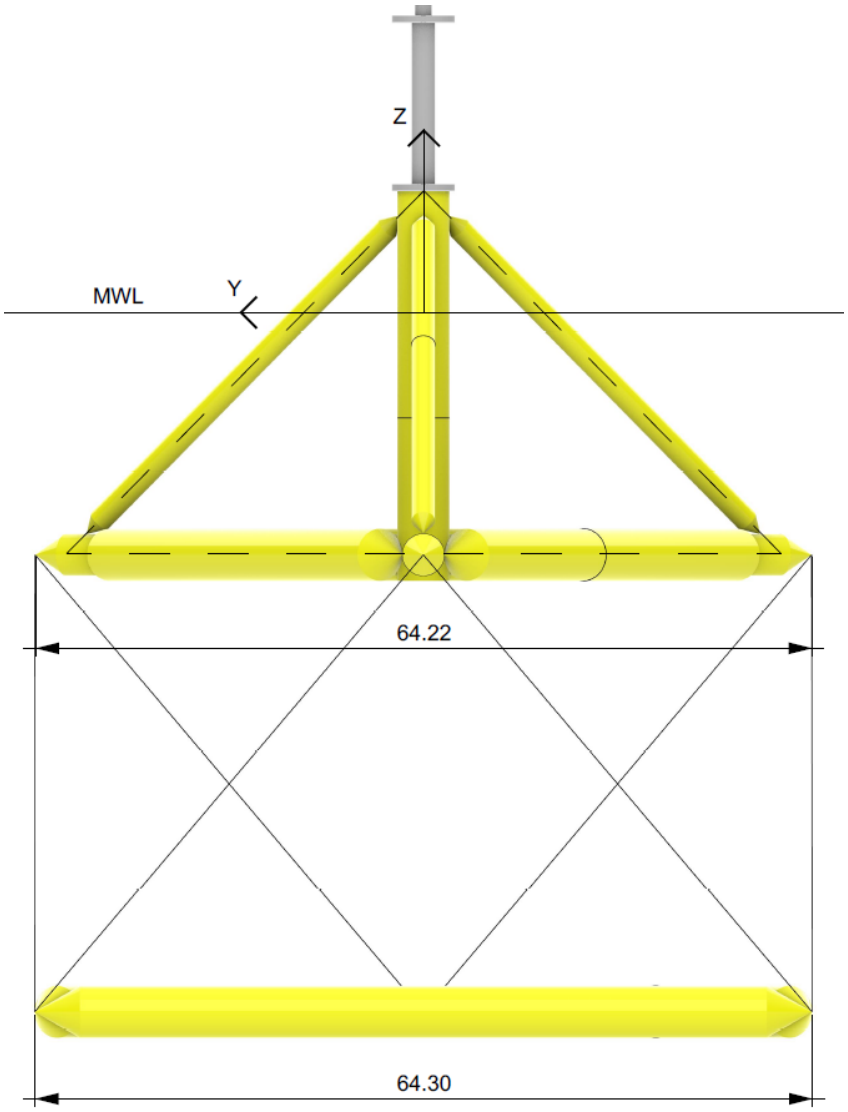

Figure 18. TetraSpar front view with full-scale dimensions

Figure 19 shows the node connections. In the physical model, the nodes were made of 3D-printed nylon and contained a pinhole for connecting the members as shown in the center image of Figure 19. For numerical modeling purposes, these nodes will be treated as simple cones, as shown in the left image of Figure 19. The angle of the modeled cone is 60°, resulting in a cross section of an equilateral triangle.

Figure 19. Node connections: left - modeled characteristic node cross section, center – experiment characteristic node (Allen and Fowler 2019), right – central column connection (Allen and Fowler 2019)

Note that all connections feature these cone-shaped nodes, except for the connections between the radial braces and the bottom of the central column. At this point, the radial braces were cut to match the circumference of the central column with a flush fit as shown in the right image of Figure 19. The top and bottom of the central column also feature a flat cap, unlike the characteristic cone end.

Cylindrical members that make up the hull and keel are made with aluminum pipe. Along with the 3D-printed nodes, there is added complexity in the construction of the keel. In order to achieve a high density in the keel with the desired mass and inertia, the keel tri braces were filled with sections of foam and steel plate.

With the complexities and uncertainties in the construction, as well as scaling challenges, it was decided to treat the hull and keel as rigid for modeling purposes. The rigid body mass and inertia properties were measured separately for the hull and keel. Inertia values were found using swing tests, and center of gravity positions were found using wedge tests. The resulting values are shown in Table 13 for the hull and Table 14 for the keel. The measured center of gravity had some offset from the geometric center in the XY-plane for both the hull and keel. It is recommended that for numerical models these measured offsets are not used. The only recommended offset is for the keel COG_X, as listed in Table 14, which was found to predict equilibrium positions that best matched the experiment.

Table 13. Full-Scale Hull Properties

	Measured	Model
Mass	1.11e6 kg	
Displaced Volume	3504 m^3	
X COG	0.1 m	0.0 m
Y COG	-0.16 m	0.0 m
Z COG	-24.80 m	
I_{XX}	3.16e8 kg-m^2	
I_{YY}	2.64e8 kg-m^2	
I_{ZZ}	4.12e8 kg-m^2	

Hull center of gravity positions are defined relative to the hull tower interface, and hull inertia values are given with respect to the hull center of gravity.

Table 14. Full-Scale Keel Properties

	Measured	Model
Mass	4.51e6 kg	
Displaced Volume	2590 m^3	
X COG	-0.29 m	-0.13 m
Y COG	-0.25 m	0.0 m
Z COG	0.0 m	
I_{XX}	1.84e9 kg-m^2	
I_{YY}	1.78e9 kg-m^2	
I_{ZZ}	2.41e8 kg-m^2	2.89e9 kg-m^2

Keel center of gravity positions are defined relative to the center of the keel, and keel inertia values are given with respect to the keel center of gravity. It is believed that there was some error in the swing test for the keel inertia about the z-axis. Given the shape of the keel, I_{ZZ} cannot be lower than I_{XX} and I_{YY}. With the measured mass and the dimensions of the keel, the theoretical limits for I_{ZZ} are a minimum of 1.55e9 kg-m^2 and a maximum of 6.22e9 kg-m^2. If the members were uniformly distributed, I_{ZZ} would be equal to 2.89e9 kg-m^2, and this value is recommended for modeling. Large yaw motion is not expected and is not of particular interest, so it is likely this value will not have significant impacts on the focus of the work.

3.3.1 Keel Lines

The scale model keel lines are made of the synthetic rope: Dyneema SK99. Properties for the lines are given in Table 15 in full scale. For modeling, these lines should include pretension; a calculated pretension is given in the table based on the keel's volume and mass. The spacing of the keel and hull in Figure 16 is based on this pretensioned condition.

Table 15. Full-Scale Keel Line Material Properties

Diameter	86.0 mm
Weight in Air	4.74 kg/m
EA	1.919e10 N
Calculated Pretension	4.24e6 N

3.4 Mooring System

The mooring system consisted of three main catenary lines. Each of these three lines was made of two different sections of chain. A lower section, running from the anchor point to near the equilibrium setdown point, was made of a heavier chain, and an upper section that connected to the TetraSpar's fairleads was made of a lighter chain. The properties of the two chain types are given in Table 16. The axial stiffness value is based on the equivalent diameter and scaled Young's modulus of steel.

Table 16. Full-Scale Mooring Chain Properties

	Dry Unit Density [kg/m]	Submerged Unit Displacement [m^3/m]	EA [N]
Lower Section	767.57	9.52e-2	8.811e11
Upper Section	143.47	1.93e-2	1.786e11

The anchor locations were fixed and documented. The upwind anchor was placed in accordance with the full design mooring system. The two downwind lines needed to be truncated due to the width of the tank; it was expected that the setdown point would never reach the truncated anchor locations in the tests. Figure 20 shows an above view of the mooring arrangement with the anchor location coordinates. The positions are relative to the origin, which is the intersection of the still free surface and the axis of the wind turbine tower.

It should be noted that the spacing of the lines is not an even 120°. The anchors of the two downwind lines are also not located at the same position in the x-direction, leading to some inherent asymmetry.

Figure 20. Mooring arrangement with full-scale anchor locations

Reported lengths of both the upper and lower sections of chain are given for each line in Table 17. Numerical models with these line lengths and corresponding mass and volume do not result in a mooring system with reactions consistent to measured values in the tests. A longer line length in the upper section needs to be used in models. This is apparent both in the resulting stiffness of the system in surge and sway, and also in visual observations of the setdown point location. Table 17 reports both the reported length of the upper sections as well as the suggested corrected lengths to use in numerical models. These suggested lengths result in fairlead tensions calculated with MoorDyn that best match the recorded values.

Table 17. Full-Scale Mooring Line Lengths

	Length [m]		
	Lower Section	Upper Section Recorded	Upper Section Corrected
Line 1	75.68	193.07	215.50
Line 2	480.96	204.47	229.22
Line 3	75.68	191.78	225.59

3.4.1 Mooring Additions

Two additional modifications were incorporated into the mooring system. The first is the inclusion of the sensor umbilical. Power and data transmission lines needed to be run from the tank carriage to the instruments on the platform. All of the lines were consolidated into a single umbilical, which was hung as a catenary line from the second flange of the tower. This was done in an effort to minimize the impact on the system's characteristics. Figure 21 shows an image of the sensor umbilical during a test. The umbilical did have a large impact on the system; the surge natural frequency, for example, was more than doubled with the added connection. The umbilical was present for all environmental load cases.

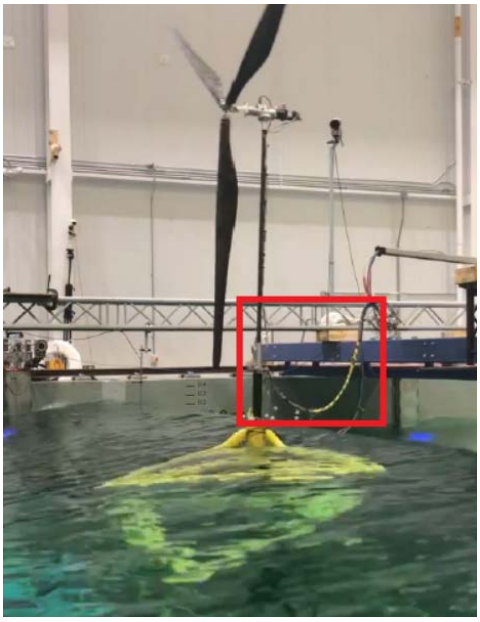

Figure 21. Sensor umbilical (Allen and Fowler 2019)

The umbilical needs to be incorporated into numerical models to match the properties of the system. Detailed knowledge about the weight and stiffness of the umbilical is not known, and the exact positioning of the cables may change throughout the test campaign. Decay tests were performed both with and without the umbilical for each degree of freedom. Numerical model implementation of the umbilical should be tuned to best match the influence observed in the decay tests.

One proposed model for the umbilical is an additional catenary mooring line connected at the second flange of the tower (0.0 m, 0.0 m, 24.68 m in the global coordinate system). The sensor

cables not only extend from the carriage to the platform, but also run along the platform to the specific sensor locations.

Table 18 provides characteristics of a proposed model, with the total additional mass distributed between the catenary portion, the tower, and the hull. The anchor point is fixed and is given with respect to the main platform coordinate system at the intersection of the mean water line and the center of the central column. The mass fractions indicate how much of the total umbilical mass should be added in each location. This is one initial suggestion, and individual tuning of the model is recommended.

It was found that with this model for the umbilical, the equilibrium position of the platform in heave and surge matched those recorded in the model tests. Further, the surge, heave, and pitch natural frequency with this total mooring system matched the natural frequency with the corresponding mooring system in the model tests. Other numerical methods to model the impact of the sensor umbilical could be implemented.

Table 18. Proposed Sensor Umbilical Catenary Model Full-Scale Properties

Umbilical Mass	152500 kg
Anchor Point X	25.0 m
Anchor Point Y	0.0 m
Anchor Point Z	40.0 m
Catenary Length	45.0 m
Catenary Mass Fraction	0.67
Tower Mass Fraction	0.02
Hull Mass Fraction	0.31

The second modification to the system was an added yaw stiffness bridle. It was found that in the extreme storm conditions, unexpected yaw motion occurred that was not representative of the physical full-scale response. University of Maine attributed this occurrence to the larger drag of the idling model-scale rotor, which featured disproportionately large chord lengths (chosen for the operating thrust characteristics). To limit the yaw motion, which was not a main subject of the study, the added yaw stiffness bridle was put in place only for the extreme storm conditions.

The yaw bridle is shown in Figure 22, highlighted in red. Two lightweight monofilament lines were connected to the same fairlead as the upwind mooring line, and run outward to the tank walls. The orientation of these lines was intended to be as close to in line with the y-axis as possible to minimize impact on surge, heave, and pitch stiffness, as well as the draft of the platform. The line connections were placed slightly downwind of the platform equilibrium position to offer the best characteristics when some surge displacement was present during environmental load cases. A series of pulleys at the tank walls directed the monofilament to soft springs outside the tank. The line length was set to have pretension in the undisplaced position. Properties of the bridle are given in full scale in Table 19, and the position of the bridle can also be seen in Figure 20. It can be assumed that the elasticity of the monofilament is insignificant compared with the soft springs.

Table 19. Yaw Stiffness Bridle Full-Scale Properties

Spring Stiffness	1.11e4 N/m
Spring Length	12.01 m
Monofilament Diameter	30.57 mm
Pretension	81.49 kN
Anchor X Location	-28.50 m
Anchor Y Location	±191.05 m
Anchor Z Location (first pulley)	-20.89 m

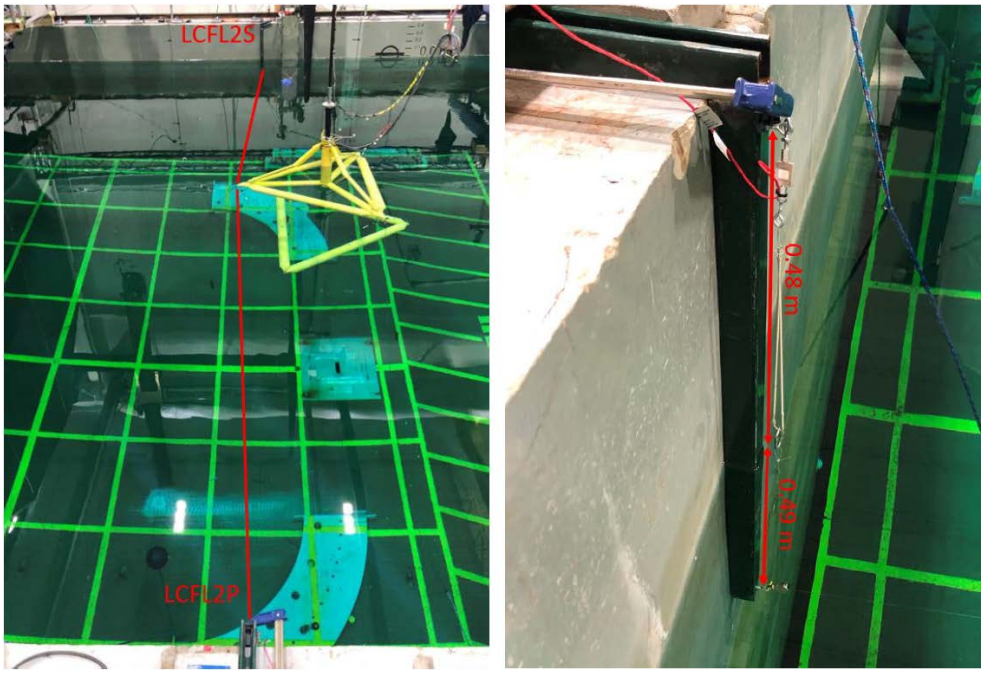

Figure 22. Yaw stiffness bridle (Allen and Fowler 2019)

A third addition to the system accounts for the mass of the keel line and fairlead tension sensors. These additional masses should be added for all load cases and can be treated as point masses at the fairlead locations, at the tip of the radial braces. The masses are given in Table 20. The sensor mass at Fairlead 2 is larger, as higher loads are expected in this mooring line, and a tension sensor with a higher limit was used.

Table 20. Full-Scale Sensor Mass Additions

Location	Total Sensor Mass
Fairlead 1	12917 kg
Fairlead 2	15699 kg
Fairlead 3	12917 kg

Offset tests were performed in both the surge and sway direction to quantify the stiffness of the system. These tests were done with three different mooring configurations: one with only the three catenary lines, one with the addition of the sensor umbilical, and a third with both the sensor umbilical and the yaw stiffness bridle. No environmental load cases were performed

without the sensor umbilical, but it is useful to consider this configuration to isolate the impact of the umbilical.

The catenary lines produce fairlead tensions that have a nonlinear relationship with body displacement. Figure 23 shows the tensions in surge and sway static offset. Fairlead 2 is the tension at the upwind fairlead, and Fairlead 1 and Fairlead 3 are the tensions at the two downwind fairleads. The dashed lines labeled "NU" are the configuration with no umbilical; note that, with this configuration, the equilibrium surge position has a much lower x-position, leading to different tested range. The dashed-dotted lines labeled "YB" are the configuration with the added yaw stiffness bridle; this addition does not significantly impact the surge stiffness or equilibrium position, but it is impactful for large sway offsets.

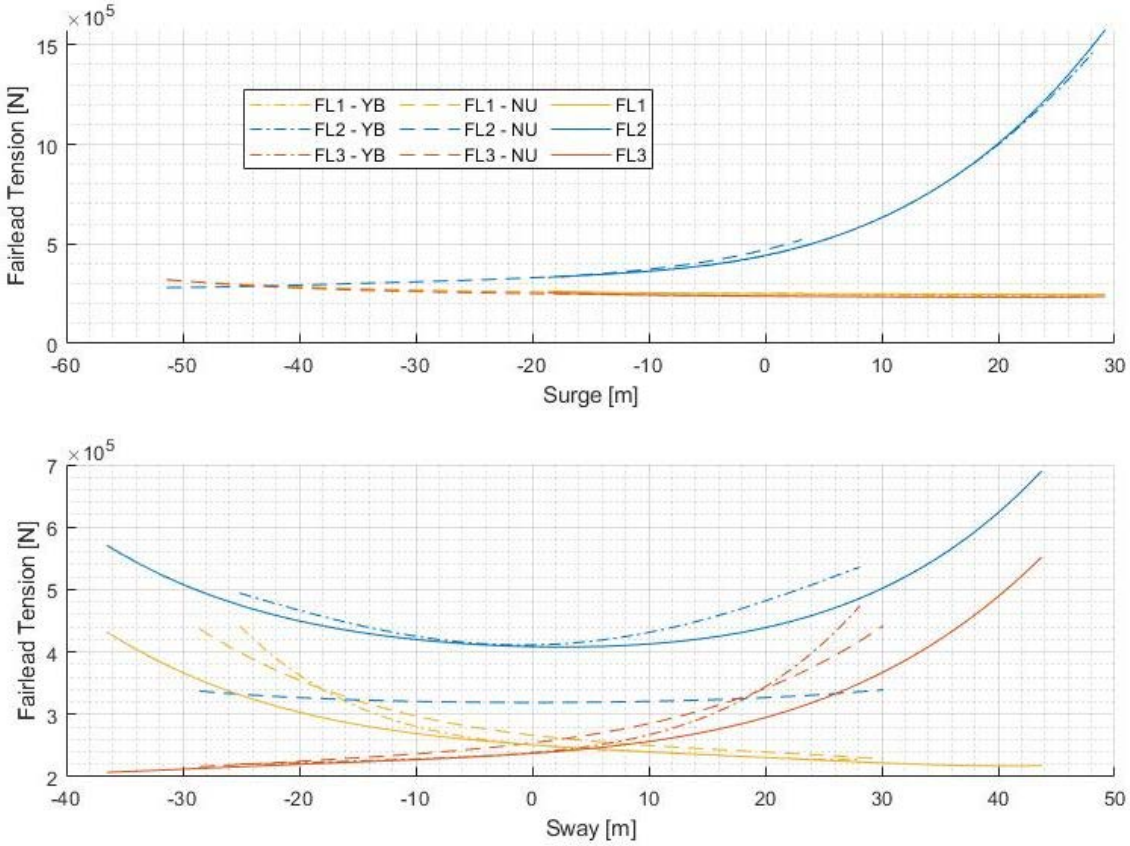

Figure 23. Full-scale mooring line loads in surge and sway static offset

In the tests, the forced motion of the platform is slow enough that the mooring lines reach a quasistatic state. The additions to the system in the different configurations are all added in parallel, so for any given position of the platform considering each degree of freedom, the load from an individual mooring component should not change. This is evident in the plot of the surge offsets. The addition of the umbilical pulls the equilibrium location higher in the x-direction, but the measured mooring loads are just an extension of the loads observed with no umbilical. The yaw bridle has a very small impact on the equilibrium surge position, and thus the range of surge locations is similar, and there is no significant difference in the measured tensions.

The change in equilibrium surge position due to the umbilical impacts the sway stiffness of each line. This is seen by the significant distance from the dotted lines to the solid and dashed lines in Figure 23. It also appears that the yaw bridle has an impact on the sway stiffness of the three main catenary lines. It is possible that this changes due to a change in the yaw, surge, or heave position of the platform during the forced sway motion. Some of the asymmetry in the system is also evident in the results of the sway offset tests. The position where the two downwind fairleads see the same tension is not at the midpoint of the tank, but instead between positive 2–4 m.

As a check for numerical mooring models, the tensions and line shapes are provided below when the platform is fixed with zero displacement in all six degrees of freedom. This case was not tested in the experiment, but can be used as a first simple check for models. The tensions are given in Table 21, and the line shapes are shown in Figure 24. These results are calculated using MoorDyn v1 within OpenFAST v3.2.1.

Table 21. Example Full-Scale Mooring Line Numerical Model Tensions

	Line 1	Line 2	Line 3
Fairlead Tension [N]	2.51e5	4.27e5	2.38e5

The shared file *Mooring_lines_visualization.fig* contains the three-dimensional line coordinates depicted in Figure 24 and can be used for model verification. Note that, when the platform is in this fixed position with no displacement, the connection between the heavy and light chains is lifted off the seabed for Line 2 but is on the seabed for Line 1 and Line 3.

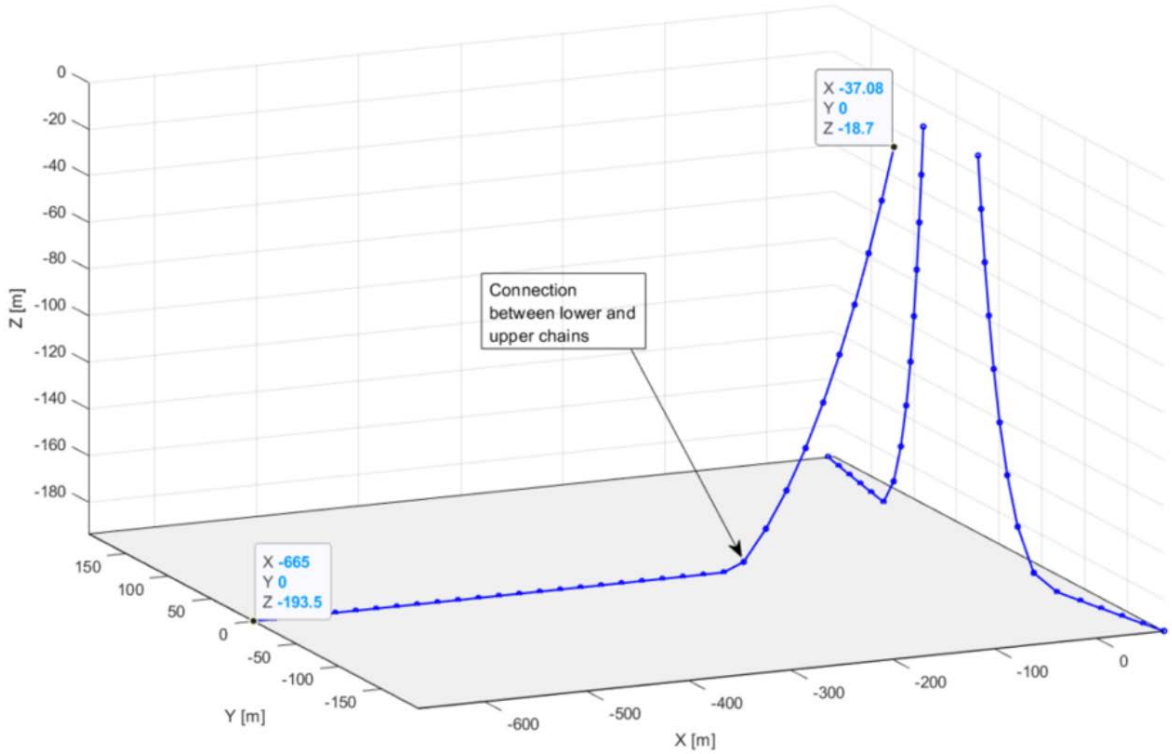

Figure 24. Example mooring line numerical model shapes

4 Simulations

Numerical modeling cases include system identification tests, which are used to check and tune the properties of the system, and environmental load cases, which are used for tool validation with comparison against the model test responses. For simplicity, all load cases will use the same output format. Table 29 explains this format, which includes 34 columns.

Simulation time step selection is open to each participant, and models should be checked to ensure the time step is sufficiently small. For consistency in reporting, all output files should use the same time step of 0.14 s. Output data should be resampled to this time step.

4.1 System Identification

4.1.1 Equilibrium and Static Offset

Load Cases 1.0–1.2 are used to evaluate the properties of the floating system and the mooring system. They are described in Table 22. Load Case 1.0 is used to make sure that the platform is stable and floating as expected. In this test, all six degrees of freedom are active, and there is no external excitation. No mooring system is present, so the test isolates the mass and buoyancy balance of the platform and turbine. The mooring system would add a significant gravity load to the platform. In order for the check to still be in roughly the same equilibrium position, a lumped mass should be added at the hull center of gravity. This mass is given in Table 22; note that the additional sensor masses in Table 20 should still be included.

In Load Case 1.1, the base mooring system is included with the umbilical but no yaw bridle. This test again checks the equilibrium position, but now with the influence of the mooring system.

Load Case 1.2 is an offset test and is used to assess the pretension and stiffness of the mooring system. The test is only performed with the base mooring system, again consisting of the three catenary lines and the sensor umbilical, but no yaw bridle. The offsets are performed to determine the stiffness in the surge direction. All six degrees of freedom are fixed and set to a prescribed value. The positions are taken from the model tests and are given in Table 23. The values are for the hull center of gravity, and are the offset displacements relative to the defined hull center of gravity position given in Table 13. Full-Scale Hull Properties. Fixing all degrees of freedom as measured isolates the impact on the fairlead tension only to the mooring system properties and not to the coupling of degrees of freedom. The desired output is the fairlead tension for each position. Participants should ensure that the reported fairlead tensions are converged values.

Table 22. Simulation Static Offset Test Matrix

Load Case	Description	Mooring System	Run Time	Notes
1.0	Equilibrium	Lumped Mass 1.73e5 kg at Hull COG (0.0 m, 0.0 m, -13.5 m)	Until steady state	Output only one final time step
1.1	Equilibrium	Base		
1.2	Surge Offset	Base		Output one final time step per position

Table 23. Surge Offset Test Hull Center of Gravity Displacements

Position #	Surge [m]	Sway [m]	Heave [m]	Roll [deg]	Pitch [deg]	Yaw [deg]
1	-18.65	-0.15	1.91	-0.13	-1.32	1.33
2	-13.33	0.25	0.88	-0.15	-1.89	-0.09
3	-8.02	0.30	0.36	-0.16	-2.28	-0.90
4	-2.71	0.09	0.12	-0.18	-2.52	-1.23
5	2.61	-0.27	-0.02	-0.20	-2.68	-1.20
6	7.92	-0.64	-0.17	-0.22	-2.79	-0.95
7	13.23	-0.87	-0.39	-0.22	-2.92	-0.62
8	18.55	-0.80	-0.68	-0.21	-3.12	-0.35
9	23.86	-0.24	-1.00	-0.18	-3.43	-0.28
10	29.17	1.02	-1.22	-0.12	-3.93	-0.57

In the output file, the column for time should be different for Load Case 1.0, Load Case 1.1, and Load Case 1.2. For each of these tests, only report one final stabilized time step. For Load Case 1.2, there should be 10 rows of data corresponding to the 10 offset positions, and the time column should be filled with the position numbers.

Table D- 1 in Surge Offset Fairlead Tensions gives the experimental fairlead tensions for each of the 10 offset positions of Load Case 1.2. These values should be used to ensure the modeled mooring system provides the appropriate stiffness.

4.1.2 Free Decay

Free-decay tests are used to help tune the properties of the numerical system. Surge, heave, and pitch are of particular interest for the analysis, so decay tests are performed to check the natural frequencies and damping values against the model test decays. Load Cases 2.1–2.3 are described in Table 24. The initial positions are regarding the degree of freedom relevant for that load case and correspond to the hull center of gravity position; this release displacement should be taken relative to the equilibrium position found in Load Case 1.1. The release displacement for all other degrees of freedom should be equal to the equilibrium positions found in Load Case 1.1. The values of the initial positions are equal to the initial positions in the physical decay tests. All degrees of freedom should be active in these tests. No incident wind or waves should be present, and the blade pitch should be set as according to Table 24.

Table 24. Simulation Free-Decay Test Matrix

Load Case	Description	Mooring System	Initial Position	Blade Pitch Set Point	Run Time [s]
2.1	Surge Decay	Base	8.77 m	90°	800
2.2	Heave Decay		8.59 m	0°	300
2.3	Pitch Decay		4.62°	90°	500

The decays in each degree of freedom are performed only with the base mooring system, which includes the sensor umbilical but no yaw bridle. The yaw bridle is not expected to have a large impact on the relevant degrees of freedom. The presence of the umbilical, however, should have a significant impact on the surge natural period, as described in Table 5. Because the environmental load cases are only to be performed with the umbilical present, this is the only configuration for which results should be reported.

4.1.3 Turbine Thrust

Load Cases 3.1–3.6 are used to check and tune the thrust properties of the numerical wind turbine. In the experiment, thrust tests were performed with the platform fully constrained. The blade pitch angle was adjusted to match the desired tower base moment, because no thrust sensor was present in the nacelle.

After the blade pitch angle was selected, wind-only tests were also conducted with the platform in the moored condition. In these model tests, the turbine thrust influences the platform surge and pitch position, in addition to the tower base moment. These data provide two additional checks to make sure models are providing a reasonable aerodynamic load.

When the platform is in an equilibrium position with no excitation, the analytical tower base moment can be calculated based only on gravity loads. This analytical prediction does not agree well with the measured moment from the sensor in the experiment. Because of this discrepancy and uncertainty, the numerical aerodynamic tuning should not be based on only tower base moment. Moored tests should be used to tune the blade pitch angle, taking into account the tower base moment, surge position, and pitch position.

Load Cases 3.1–3.6 are described in Table 25, each with steady and uniform wind. The load cases should be run until the transient is gone and stabilized loads and conditions are reached. For the first three load cases, the platform should be free in each degree of freedom with the relevant mooring system, matching the conditions of the wind-only model tests. The tuned blade pitch angle that was found in the experiment is given and should be used as a starting point. The blade pitch angle should then be tuned to best balance the target tower base moment, hull surge position, and hull pitch position given in Table 26.

Load Cases 3.4–3.6 then add another verification to the turbine tuning. These load cases include the same three wind inputs and should use the blade pitch angles determined from the corresponding Load Cases 3.1–3.3. The tests isolate the impact of the wind loading, allowing a more direct comparison between the participant's turbine models. The platform should be fixed in each degree of freedom, but the tower should still be flexible.

Table 25. Simulation Turbine Thrust Test Matrix

Load Case	Description	Wind Speed [m/s]	Rpm	Blade Pitch Starting Point [deg]	Mooring
3.1	Rated	9.89	12.2	-6.2	Base
3.2	Post-Rated	24.05	13.3	18.7	Base
3.3	50-yr Storm	44.62	Idle	89	Yaw Bridle
3.4	Rated	9.89	12.2	Use Angle from Load Cases 3.1–3.3	Fixed Platform
3.5	Post-Rated	24.05	13.3		
3.6	50-yr Storm	44.62	Idle		

The target surge positions in Table 26 are absolute values, but the target values for the bending moment and pitch position are relative to the initial conditions from the experiment. This is how the tuning in Load Cases 3.1–3.3 should be performed as well. The initial conditions for the experimental bending moment and pitch position are also given as a reference. There is hesitancy to use the absolute values for the tower base moment data. This is highlighted by positive initial values in the wind-only tests. Before any wind or waves are present, the turbine overhang leads to a negative pitch value, which should result in a negative fore-aft bending moment at the tower base. Given some variability in the equilibrium pitch position between simulations and the experiment, a relative value for the target pitch position is also used.

Table 26. Thrust Target Values and Experimental Initial Conditions

Load Case	Target My [N-m] (relative)	Target Hull Surge [m] (absolute)	Target Hull Pitch [deg] (relative)	Experiment Initial My [N-m]	Experiment Initial Pitch [deg]
3.1	7.43e7	20.76	6.83	2.26e6	-1.99
3.2	2.79e7	13.35	2.49	9.31e5	-1.60
3.3	2.17e7	10.27	2.26	1.20e6	-1.60

4.2 Environmental Load Cases

Load Cases 4.1–4.4 describe the wave-only simulations, and Load Cases 5.1–5.4 describe the combined wind and wave simulations. If participants have the capability to utilize wave elevation and wind speed time series for environmental condition generation, provided data from the model tests should be used in place of statistical values. These time series are available at: https://a2e.energy.gov/ds/oc6/oc6.phase4. Note that the wave calibration data was recorded at a position 21.2 m downwind of the defined modeling origin. Time series from the wave calibration runs can be used for all wave conditions. For the regular waves in Load Case 4.1 and Load Case 5.1, if a participant cannot incorporate the recorded time series, the phase should result in a wave crest at initialization (t = 0.0 s) for consistent post-processing. The wind calibration time series from the turbulent 50-yr storm condition can be used directly. The wind calibration for the rated and post-rated conditions was not run for as long as the load cases; an artificial time series with

repetition of the calibration time series is provided for numerical modeling. The statistical values associated with all tests are given in Table 27 and Table 28.

Table 27. Simulation Wave-Only Test Matrix

Load Case	Description	Wave Spectrum	Wave Height [m]	Period [s]	γ Tor.	Γ JON.	Mooring	Duration [s]
4.1	Post-Rated	Regular	8.31	12.41	-	-	Base	3,934
4.2	Rated	Torsethaugen	1.46	6.73	2.7	2.3		10,977
4.3	Post-Rated	Torsethaugen	8.00	12.48 (12.20)	2.7	2.2		10,977
4.4	50-yr Storm	Torsethaugen	12.81	15.79	3.9	3.3	Yaw Bridle	10,977

For Load Cases 4.2–4.4 with irregular waves, the listed wave height is the significant wave height, and the listed period is the peak period. It was found that for the irregular post-rated waves (Load Case 4.3), a slightly lower peak period than reported best matched the recorded wave spectrum. A peak period of 12.2 s is recommended when reproducing the spectrum in this load case. The peak enhancement factor, γ, is also listed for these cases. The Torsethaugen wave spectrum often features two peak periods, but in this case, each wave condition only has a single peak. Equation 1 is a simplified version of the Torsethaugen wave spectrum that was developed with data from the Norwegian continental shelf (Torsethaugen and Haver 2004). Note that custom values for the peak enhancement factor are used to match the conditions of the model tests, rather than the Torsethaugen formulation for γ.

$$S(f) = \frac{{H_s}^2 T_p}{16}\ 3.26\ \frac{(1 + 1.1\ (\ln[\gamma])^{1.19})}{\gamma}(f\ T_p)^{-4} e^{-(f\ T_p)^{-4}} \gamma^{e^{-\left(\frac{(f\ Tp-1)^2}{2\ \sigma^2}\right)}}$$

Equation 1. Simplified Torsethaugen wave spectrum

H_s and T_p are the significant wave height and peak period for the wave condition. σ is the spectral width parameter and has a value of 0.07 for all frequencies below the peak frequency and a value of 0.09 for all frequencies above the peak frequency (Torsethaugen and Haver 2004).

If participants are only able to use a JONSWAP wave spectrum, slightly lower values of γ are suggested. These values are also provided in Table 27. Figure 25 shows recorded spectra for the three irregular wave conditions with the corresponding simplified Torsethaugen and JONSWAP spectra.

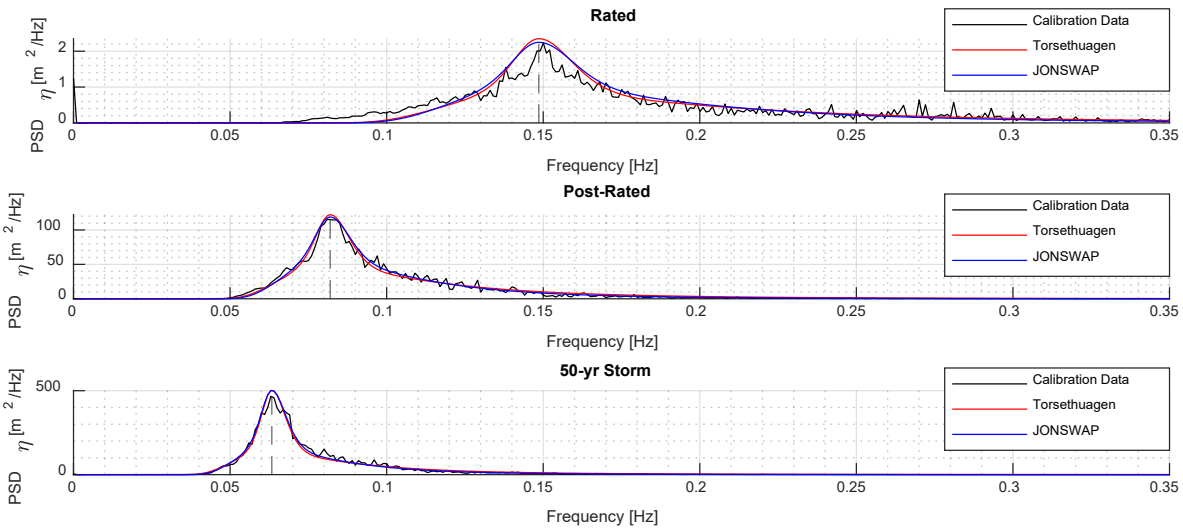

Figure 25. Recorded and optional simplified statistical wave spectra

A form of the Norwegian Petroleum Directorate wind spectrum was used in the experiment with no shear profile (Allen and Fowler 2019). Only the extreme 50-yr storm load case featured a turbulent inflow wind; in the rated and post-rated cases, a steady wind was used. For numerical modeling, a time series of the measured hub-height wind speed in the x-direction is provided. In a Floating Offshore-wind and Controls Advanced Laboratory experiment, also conducted in the University of Maine's W2 basin, it was found that a spatially uniform model best matched the experiment (Mendoza et al. 2022). Load Cases 5.1–5.4 should follow these findings and use a spatially uniform wind field with the provided velocity time series.

Table 28. Simulation Wind and Wave Test Matrix

Load Case	Description	Wave Spectrum	Wave Height [m]	Wave Period [s]	Wind Speed [m/s]	Turbulence Intensity	Mooring	Duration [s]
5.1	Post-Rated	Regular	8.31	12.41	24.05	2.51%	Base	3934
5.2	Rated	Torsethaugen	1.46	6.73	9.89	2.40%		10977
5.3	Post-Rated	Torsethaugen	8.00	12.48 (12.20)	24.05	2.51%		10977
5.4	50-yr Storm	Torsethaugen	12.81	15.79	45.22	8.89%	Yaw Bridle	10977

Table 29 lists all of the desired outputs for Load Cases 1.1–5.4. The transient phase should be removed from the output when applicable. For consistency in post-processing, all submitted files should follow a standard naming convention (e.g., *NAME_LC12.txt*). Each participant should choose up to four letters to represent their institution (*NAME*). For participants using different modeling approaches, the name should be followed by a single number indicating the modeling approach (*NAME1 and NAME2*). The last two numbers of the file name indicate the load case (12 is for Load Case 1.2).

The output should be a space delimited text file with 34 columns, following the convention in Table 29. Two header rows are optional for clarity, the first row should have the OC6 variable name, and the second row should have the variable unit. If one or both of these header rows are not present, the data can still be processed.

Table 29. Environmental Load Case Output List

Column	Description	OC6 Name	University of Maine Name	Unit	Notes
1	Physical Time (Position for static offset tests)	Time	Time	s	
2	Wind Speed	WindVxi	WindCalX	m/s	At hub height
3	Wave Elevation	WaveElev	WaveCal3	m	WaveElev at (0,0) m WaveCal3 at (21.2,-1.3) m
4	Tower Base Fore-Aft Bending Moment	TowerMy	TowerMy	N-m	
5	Tower Base Side-Side Bending Moment	TowerMx	TowerMx	N-m	
6	Rotor Speed	Rpm	RotorSpeed	rpm	
7	Tower Top X Acceleration	AccTx	AccTx	m/s^2	
8	Tower Top Y Acceleration	AccTy	AccTy	m/s^2	
9	Tower Top Z Acceleration	AccTz	AccTz	m/s^2	
10	Hull Surge Position	HullSurge	HullCOGX	m	Position of the hull is with respect to the hull center of gravity
11	Hull Sway Position	HullSway	HullCOGY	m	
12	Hull Heave Position	HullHeave	HullCOGZ	m	
13	Hull Roll Position	HullRoll	HullCOGRX	deg	
14	Hull Pitch Position	HullPitch	HullCOGRY	deg	
15	Hull Yaw Position	HullYaw	HullCOGRZ	deg	
16	Keel Surge Position	KeelSurge	KeelCOGX	m	Position of the keel is with respect to the keel center of gravity
17	Keel Sway Position	KeelSway	KeelCOGY	m	
18	Keel Heave Position	KeelHeave	KeelCOGZ	m	
19	Keel Roll Position	KeelRoll	KeelCOGRX	deg	
20	Keel Pitch Position	KeelPitch	KeelCOGRY	deg	
21	Keel Yaw Position	KeelYaw	KeelCOGRZ	deg	
22	Fairlead 1 Tension	FL1T	LCFL1	N	
23	Fairlead 2 Tension	FL2T	LCFL2	N	
24	Fairlead 3 Tension	FL3T	LCFL3	N	
25	Keel Line 1 Tension	KL1T	LCSL1T	N	
26	Keel Line 2 Tension	KL2T	LCSL2T	N	
27	Keel Line 3 Tension	KL3T	LCSL3T	N	
28	Keel Line 4 Tension	KL4T	LCSL4T	N	
29	Keel Line 5 Tension	KL5T	LCSL5T	N	
30	Keel Line 6 Tension	KL6T	LCSL6T	N	
31	Yaw Bridle Tension 1	YB1T	LCFL2S	N	Only for 50-yr Storm Cases
32	Yaw Bridle Tension 2	YB2T	LCFL2P	N	
33	Aerodynamic Rotor X Force	AFx	N/A	N	
34	Blade Pitch Angle	BldPitch	N/A	deg	

References

Allen, C., & Fowler, M. (2019). *1/43rd Scale Basin Testing of the 3.6 MW TetraSpar Floating Offshore Wind Turbine - Spar Configuration.* Advanced Structures and Composites Center. University of Maine.

Mendoza, Robertson, Wright, Jonkman, Wang, Bergua, . . . Viselli. (2022, October). Verification and Validation of a Model-Scale Turbine Performance and Control Strategies for the IEA Wind 15 MW Reference Wind Turbine. *Energies*(Numerical Analysis, Field Testing and Experimental Assessment of Offshore Wind Turbines 2022).

SOT. (2021, December). *The TetraSpar full-scale demonstration project*. Retrieved from Stiesdal: https://www.stiesdal.com/offshore-technologies/the-tetraspar-full-scale-demonstration-project/

Torsethaugen, K., & Haver, S. (2004). *Simplified Double Peak Spectral Model for Ocean Waves.* Trondheim, Norway: SINTEF.

Appendix A. Instruments

Table A-1. Model Test Sensor Details (Allen and Fowler 2019)

Channel Name	Units	Froude Scale Factor	Description	Sensor	AS#	Notes
Time	Sec	6.56	Time Stamp	Synchronization Clock	N/A	
WaveProbeRef1	m	43.00	Wave Reference Probes	Akamina Technologies, AWP-24-3	N/A	Left installed for calibration and testing.
WaveProbeRef2	m	43.00			N/A	Left installed for calibration and testing.
WaveProbeRef3	m	43.00			N/A	Left installed for calibration and testing.
WaveProbeRef4	m	43.00			N/A	Left installed for calibration and testing.
WaveProbeRef5	m	43.00			N/A	Left installed for calibration and testing.
WaveProbeRef6	m	43.00			N/A	Left installed for calibration and testing.
WaveCal1	m	43.00	Wave Calibration Probes	Edinburgh Wave Probes	N/A	Removed after calibration.
WaveCal2	m	43.00			N/A	Removed after calibration.
WaveCal3	m	43.00			N/A	Removed after calibration.
AirRef	m/s	6.56	Wind Reference Probe	TSI Incorporated, Hotwire model 8455-06	AS2102	Wind speed magnitude.
WindCalX	m/s	6.56	Wind Calibration Probe	RM Young 81000	AS2340	Ultrasonic anemometer, measures 3 direction wind velocity, removed after calibration.
WindCalY	m/s	6.56				
WindCalZ	m/s	6.56				
Torque	Nm	3504271.03	Turbine LSS Torque	Interface T4-10-B1A	AS2234	
AccTx	g	1.00	Tower Top Accelerations	PCB Piezotronics Model 356A17	AS2083	
AccTy	g	1.00				
AccTz	g	1.00				
AccBx	g	1.00	Tower Base Accelerations	PCB Piezotronics Model 356A17	AS2084	Signal with instrument was hindered by water damage sustained after Pink Noise cases on 12/19/28. Additional water proofing was added but signal never recovered.
AccBy	g	1.00				
AccBz	g	1.00				
LCFL2	N	81494.68	Fairlead Tensions	Futek LSB210 25lb 5lb 5lb	AS2125	
LCFL1	N	81494.68			AS2328	
LCFL3	N	81494.68			AS2093	
TowerMx	Nm	3504271.03	Tower Base Moments	Calibrated strain array	N/A	
TowerMy	Nm	3504271.03			N/A	
LCSL1T	N	81494.68	Tendon Tensions	Customer provided instrumentation. HBM U9C, 100N	N/A	SOT1
LCSL6T	N	81494.68				SOT2
LCSL5T	N	81494.68				SOT3
LCSL4T	N	81494.68				SOT4
LCSL3T	N	81494.68				SOT5
LCSL2T	N	81494.68				SOT6

Channel Name	Units	Froude Scale Factor	Description	Sensor	AS#	Notes
SGRB2B-AXIAL	mV/v	1.00	Hull Strain Gauges	Customer provided instrumentation. Tokyo Sokki Kenkyuho Co. WFLA-6-5L-11	N/A	
SGRB2B-TRANS	mV/V	1.00	Hull Strain Gauges			
SGRB2T-AXIAL	mV/V	1.00	Hull Strain Gauges			
SGRB2T-TRANS	mV/V	1.00	Hull Strain Gauges			
SGRB1B-AXIAL	mV/V	1.00	Hull Strain Gauges			
SGRB1T-TRANS	mV/V	1.00	Hull Strain Gauges			Lost meaningful signal with the instrument starting with initial tests on 1/9/19. Sensor was not replaced due to inaccessibility.
LCFL2P	N	81494.68	Additional Mooring Fairlead Tensions	Futek LSB210 10lb	AS2650	Added later for additional Yaw stiffness
LCFL2S	N	81494.68		10lb	AS2074	Added later for additional Yaw stiffness
Rotor Speed	RPM	0.15	Rotor Speed	Parker Motor BE164DJ-NFON Encoder	N/A	For conditions where the turbine was set to free rotor speed could not be measured since the motor was not turned on. For these conditions "NaN" values are found in the data.
Nac X	m	43.00	Nacelle Positions and Rotations	Camera Optical Tracking Array Above Water: Oqus 5+, 4MP, Infrared Strobe, Passive Markers. Underwater: Oqus 7+, 12MP, Infrared Strobe, Passive Markers	N/A	System calibrated daily.
Nac Y	m	43.00				
Nac Z	m	43.00				
Nac RX	deg	1.00				
Nac RY	deg	1.00				
Nac RZ	deg	1.00				
Keel COG X	m	43.00	Keel COG Positions and Rotations			
Keel COG Y	m	43.00				
Keel COG Z	m	43.00				
Keel COG RX	deg	1.00				
Keel COG RY	deg	1.00				
Keel COG RZ	deg	1.00				
Hull COG X	m	43.00	Hull COG Positions and Rotations			
Hull COG Y	m	43.00				
Hull COG Z	m	43.00				
Hull COG RX	deg	1.00				
Hull COG RY	deg	1.00				
Hull COG RZ	deg	1.00				
Paddle1	deg	1.00	Wave maker paddle positions	Edinburgh paddle encoder	N/A	Beginning with Paddle1, located on the +Y side of the tank as defined in Figure 6, the paddle designation increase sequentially to the –Y side of the tank.
Paddle2	deg	1.00				
Paddle3	deg	1.00				
Paddle4	deg	1.00				
Paddle5	deg	1.00				
Paddle6	deg	1.00				
Paddle7	deg	1.00				
Paddle8	deg	1.00				
Paddle9	deg	1.00				

Paddle10	deg	1.00				Please see Figure 49 for orientation definition.
Paddle11	deg	1.00				
Paddle12	deg	1.00				
Paddle13	deg	1.00				
Paddle14	deg	1.00				
Paddle15	deg	1.00				
Paddle16	deg	1.00				

Appendix B. Blade and Airfoil

Table B-1. AG04MOD Airfoil Aerodynamic Coefficients (Allen and Fowler 2019)

α [deg]	C_L	C_D
-180	0.0000	0.0625
-170	0.4660	0.0993
-160	0.4280	0.2053
-150	0.4650	0.3674
-140	0.4840	0.5656
-130	0.4620	0.7755
-120	0.3960	0.9710
-110	0.2890	1.1278
-100	0.1520	1.2261
-90	0.0000	1.2530
-80	-0.1692	1.2261
-70	-0.3193	1.1278
-60	-0.4360	0.9710
-50	-0.5087	0.7755
-40	-0.5350	0.5656
-30	-0.5184	0.3674
-20	-0.4825	0.2053
-10	-0.5208	0.0992
-9	-0.5199	0.0880
-8	-0.5166	0.0765
-7	-0.5100	0.0650
-6	-0.4993	0.0537
-5	-0.4838	0.0428
-4.5	-0.4277	0.0378
-4	-0.3713	0.0341
-3.5	-0.3149	0.0310
-3	-0.2584	0.0285
-2.5	-0.2017	0.0265
-2	-0.1451	0.0249
-1.5	-0.0883	0.0237
-1	-0.0314	0.0228
-0.5	0.0255	0.0218
0	0.0824	0.0221
0.5	0.1393	0.0220
1	0.1963	0.0221
1.5	0.2532	0.0224
2	0.3101	0.0231
2.5	0.3669	0.0239
3	0.4237	0.0252
3.5	0.4804	0.0265
4	0.5370	0.0282
4.5	0.5935	0.0305
5	0.6500	0.0338
5.5	0.7063	0.0382
6	0.7625	0.0422
6.5	0.7619	0.0495
7	0.7603	0.0625
7.5	0.7579	0.0807
8	0.7544	0.0926
8.5	0.7500	0.1019
9	0.7456	0.1099
9.5	0.7423	0.1179
10	0.7410	0.1270
11	0.7482	0.1482
12	0.7679	0.1708
13	0.7970	0.1946
14	0.8322	0.2191
15	0.8706	0.2441
16	0.9090	0.2693
17	0.9442	0.2943
18	0.9733	0.3188
19	0.9930	0.3425
20	1.0002	0.3650
25	0.9534	0.4683
30	0.8794	0.5668
35	0.8284	0.6597
40	0.7807	0.7487
45	0.7354	0.8359
50	0.6890	0.9183
60	0.5803	1.0627
70	0.4187	1.1705
80	0.2183	1.2351
90	0.0000	1.2530
100	-0.1520	1.2261
110	-0.2890	1.1278
120	-0.3960	0.9710
130	-0.4620	0.7755
140	-0.4840	0.5656
150	-0.4650	0.3674
160	-0.4280	0.2053
170	-0.4660	0.0993
180	0.0000	0.0625

Table B-2. Cylinder Airfoil Aerodynamic Coefficients (Allen and Fowler 2019)

α [deg]	C_L	C_D
-180	0.0000	0.5000
-170	0.0000	0.5000
-160	0.0000	0.5000
-150	0.0000	0.5000
-140	0.0000	0.5000
-130	0.0000	0.5000
-120	0.0000	0.5000
-110	0.0000	0.5000
-100	0.0000	0.5000
-90	0.0000	0.5000
-80	0.0000	0.5000
-70	0.0000	0.5000
-60	0.0000	0.5000
-50	0.0000	0.5000
-40	0.0000	0.5000
-30	0.0000	0.5000
-20	0.0000	0.5000
-10	0.0000	0.5000
-9	0.0000	0.5000
-8	0.0000	0.5000
-7	0.0000	0.5000
-6	0.0000	0.5000
-5	0.0000	0.5000
-4.5	0.0000	0.5000
-4	0.0000	0.5000
-3.5	0.0000	0.5000
-3	0.0000	0.5000
-2.5	0.0000	0.5000
-2	0.0000	0.5000
-1.5	0.0000	0.5000
-1	0.0000	0.5000
-0.5	0.0000	0.5000
0	0.0000	0.5000
0.5	0.0000	0.5000
1	0.0000	0.5000
1.5	0.0000	0.5000
2	0.0000	0.5000
2.5	0.0000	0.5000
3	0.0000	0.5000
3.5	0.0000	0.5000
4	0.0000	0.5000
4.5	0.0000	0.5000
5	0.0000	0.5000
5.5	0.0000	0.5000
6	0.0000	0.5000
6.5	0.0000	0.5000
7	0.0000	0.5000
7.5	0.0000	0.5000
8	0.0000	0.5000
8.5	0.0000	0.5000
9	0.0000	0.5000
9.5	0.0000	0.5000
10	0.0000	0.5000
11	0.0000	0.5000
12	0.0000	0.5000
13	0.0000	0.5000
14	0.0000	0.5000
15	0.0000	0.5000
16	0.0000	0.5000
17	0.0000	0.5000
18	0.0000	0.5000
19	0.0000	0.5000
20	0.0000	0.5000
25	0.0000	0.5000
30	0.0000	0.5000
35	0.0000	0.5000
40	0.0000	0.5000
45	0.0000	0.5000
50	0.0000	0.5000
60	0.0000	0.5000
70	0.0000	0.5000
80	0.0000	0.5000
90	0.0000	0.5000
100	0.0000	0.5000
110	0.0000	0.5000
120	0.0000	0.5000
130	0.0000	0.5000
140	0.0000	0.5000
150	0.0000	0.5000
160	0.0000	0.5000
170	0.0000	0.5000
180	0.0000	0.5000

Table B-3. AG04 Foil Definition (Allen and Fowler 2019)

x/chord	y/chord (suction)	y/chord (pressure)
1	0.0046	-0.0046
0.975	0.0079	-0.0058
0.95	0.011	-0.0069
0.9	0.0173	-0.009
0.85	0.0236	-0.0111
0.8	0.0298	-0.0133
0.75	0.0358	-0.0156
0.7	0.0418	-0.0181
0.65	0.0477	-0.0209
0.6	0.0535	-0.0241
0.55	0.059	-0.0274
0.5	0.0642	-0.031
0.45	0.0688	-0.0346
0.4	0.0728	-0.0382
0.35	0.0759	-0.0416
0.3	0.0779	-0.0447
0.25	0.0786	-0.047
0.2	0.0774	-0.0484
0.15	0.0734	-0.0482
0.1	0.0652	-0.0453
0.075	0.0586	-0.042
0.05	0.0492	-0.0366
0.025	0.035	-0.0273
0.0125	0.0242	-0.0195
0.0075	0.0182	-0.015
0.005	0.0148	-0.0123
0.0025	0.0097	-0.0084
0.001	0.0056	-0.0054
0	0	0

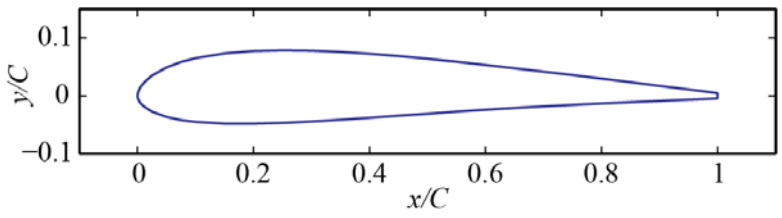

Figure B-1. AG04 foil shape (Allen and Fowler 2019)

Table B-4. Blade Properties (Allen and Fowler 2019)

Radial Position [m]	Angle of Twist [deg]	Chord Length [m]	Section Shape	Thickness/Chord
0.00	33.46	2.24	Cylinder	1
1.70	33.46	2.24	Cylinder	1
2.41	30.07	2.92	Blend	-
5.16	20.07	3.66	Blend	-
8.80	12.76	4.73	Blend	-
11.19	9.95	5.29	Blend	-
13.50	8.03	5.55	Blend	-
16.01	6.51	5.63	Blend	-
18.29	5.45	5.55	AG04MOD	0.118
20.67	4.58	5.38	AG04MOD	0.118
23.05	3.88	5.12	AG04MOD	0.118
25.44	3.31	4.82	AG04MOD	0.118
27.82	2.83	4.47	AG04MOD	0.118
30.20	2.43	4.13	AG04MOD	0.118
32.58	2.08	3.83	AG04MOD	0.118
34.97	1.78	3.57	AG04MOD	0.118
37.35	1.51	3.35	AG04MOD	0.118
39.74	1.28	3.14	AG04MOD	0.118
42.12	1.07	2.97	AG04MOD	0.118
44.51	0.88	2.84	AG04MOD	0.118
46.90	0.72	2.67	AG04MOD	0.118
49.30	0.57	2.54	AG04MOD	0.118
51.69	0.43	2.45	AG04MOD	0.118
53.93	0.31	2.32	AG04MOD	0.118
55.79	0.22	2.24	AG04MOD	0.118
57.37	0.15	2.19	AG04MOD	0.118
58.77	0.09	2.02	AG04MOD	0.118
59.80	0.04	1.85	AG04MOD	0.118
60.33	0.02	1.59	AG04MOD	0.118
60.57	0.01	1.42	AG04MOD	0.118
60.90	0.00	0.82	AG04MOD	0.118
61.10	0.00	0.00	AG04MOD	0.118

* Thickness-to-chord ratios and airfoil coefficients for the blended sections should be linearly interpolated between the last cylindrical root section and the first AG04MOD section based on radial position.

Appendix C. Platform Coordinates

Figure C-1 shows the locations of the joints (SOT 2021). For modeling purposes, the platform is treated as symmetric about the X-Z plane. Joints mirrored about this plane have the same x and z coordinates and opposite y coordinates.

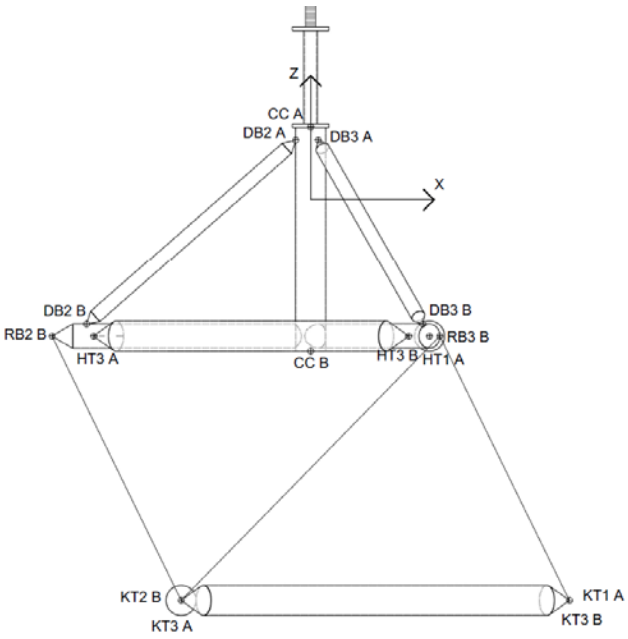

Figure C-1. TetraSpar joint coordinate locations

Table C-1. TetraSpar Joint Coordinates

	Coordinate [m]		
	X	Y	Z
CC A	0.00	0.00	11.30
CC B	0.00	0.00	-20.85
RB2 B	-37.08	0.00	-18.70
RB3 B	18.54	-32.11	-18.70
HT1 A	17.05	-26.09	-18.70
HT3 A	-31.12	-1.72	-18.70
HT3 B	14.07	-27.81	-18.70
DB2 A	-2.15	0.00	9.41
DB2 B	-32.15	0.00	-16.98
DB3 A	1.08	-1.86	9.41
DB3 B	16.07	-27.84	-16.98
KT1 A, KT3 B	37.12	0.00	-56.60
KT2 B, KT3 A	-18.56	-32.15	-56.60

Appendix D. Surge Offset Fairlead Tensions

Table D-1. Model Test Fairlead Tensions at Surge Offset Positions

	Fairlead Tension [10^5 N]		
Position #	Line 1	Line 2	Line 3
1	2.636	3.326	2.545
2	2.572	3.495	2.477
3	2.534	3.733	2.431
4	2.513	4.131	2.399
5	2.500	4.788	2.374
6	2.492	5.802	2.354
7	2.484	7.286	2.338
8	2.476	9.359	2.329
9	2.468	12.135	2.333
10	2.462	15.746	2.358